Spectroscopy of third-harmonic generation: evidence for resonances in model compounds and ligated hemoglobin

G. Omar Clay

Department of Physics, University of California at San Diego, La Jolla, California 92093

Andrew C. Millard*

Department of Chemistry and Biochemistry, University of California at San Diego, La Jolla, California 92093

Chris B. Schaffer†

Department of Physics, University of California at San Diego, La Jolla, California 92093

Juerg Aus-der-Au‡

Department of Electrical and Computer Engineering, University of California at San Diego, La Jolla, California 92093

Philbert S. Tsai

Department of Physics, University of California at San Diego, La Jolla, California 92093

Jeffrey A. Squier**

Department of Electrical and Computer Engineering, University of California at San Diego, La Jolla, California 92093

David Kleinfeld

Department of Physics, University of California at San Diego, La Jolla, California 92093

Received September 2, 2005; revised November 17, 2005; accepted November 18, 2005; posted November 29, 2005 (Doc. ID 64600)

We report on third-harmonic generation (THG) of biomolecular solutions at the fluid/glass interface as a means to probe resonant contributions to their nonlinear absorption spectra that could serve as contrast mechanisms for functional imaging. Our source was 100 fs laser pulses whose center wavelength varied from 760 to 1000 nm. We find evidence of a two-photon resonance in the ratio of third-order susceptibilities, $\chi^{(3)}_{\text{sample}}(3\omega)/\chi^{(3)}_{\text{glass}}$, for aqueous solutions of Rhodamine B, Fura-2, and hemoglobin and a three-photon resonance in $\chi^{(3)}_{\text{sample}}(3\omega)/\chi^{(3)}_{\text{glass}}$ for solutions of bovine serum albumin. Consistent with past work, we find evidence of a one-photon resonance of $\chi^{(3)}_{\text{sample}}(3\omega)/\chi^{(3)}_{\text{glass}}$ for water, while confirming a lack of resonant enhancement for benzene. At physiological concentrations, hemoglobin in different ligand-binding states could be distinguished on the basis of features of its THG spectrum.

OCIS codes: 190.4160, 190.4180, 190.4350, 190.4710, 300.6420, 170.3880, 120.6200.

1. INTRODUCTION

The nonlinear spectroscopy of fluids has assumed new relevance with the advent and proliferation of nonlinear microscopies.[1] In these techniques, an ultrashort pulse of laser light is tightly focused into a material so that optical excitation is confined to a focus where the photon flux is highest. This provides intrinsic three-dimensional optical sectioning for two-photon laser scanning microscopy,[2–4] second-harmonic generation,[5] three-photon laser scanning microscopy,[6–9] and third-harmonic generation[10–14] (THG). Whereas contrast in two-photon and three-photon scanning microscopy is typically achieved through the use of fluorescent indicators, contrast in harmonic generation relies almost exclusively on intrinsic chromophores. *A priori*, THG will depend directly on one-, two-, and three-photon absorption resonances[15] and thus may be expected to report changes in the function properties of biologically active molecules. An understanding of the nonlinear resonant properties is of further importance as a means to indicate pathways for phototoxicity and shadowing by multiphoton absorption.

Under tight focusing conditions, the extent of THG in-

creases dramatically when the focus spans an interface between two optically different materials.[10,16] This allows imaging based on THG to resolve otherwise transparent interfaces and inhomogeneities within the resolution of the confocal parameter and without the use of dyes.[11,13,17–19] Mitochondria,[20] red blood cells,[21,22] embryonic development,[18,23] neurons,[13] plasma flows,[24,25] muscle fibers,[26] and skin biopsy samples[27] have been visualized in this manner. Third-harmonic imaging contrast has also been linked to the density of optical solids,[24] the aggregation state of polymers,[28–30] and the concentration of intracellular calcium in cultured human glial cells.[31] Finally, a near-field THG scanning imaging study of a dried red blood cell by Schaller *et al.*[22] qualitatively showed that their image contrast was best when their excitation beam was spectrally tuned near an anticipated three-photon resonance in hemoglobin. This past work motivates the need for a systematic study of possible functional THG signals.

Beyond issues of imaging, nonlinear optical spectroscopy *per se* provides insight into the structure and electronic properties of materials that is complementary to that provided by linear spectroscopy.[32–38] Over the past two decades, THG has emerged as a useful nonlinear spectroscopy tool[39–43] that has been widely used to identify two- and three-photon resonances in solids and thin films.[29,35,37,38,44–48] In addition, this work indicates a sensitive THG dependence on the molecular structures and interactions of solutes and solvents.[49–51]

Here we report on THG at the solution/glass interface as a means to explore the contribution of electronic resonances to THG spectra of solution-phase biocompounds. We first consider several model solutions with known one- and two-photon absorption spectra as a means to calibrate our methodology.[52–55] We then focus on physiological solutions of bovine serum albumin (BSA) as well as different ligation states of hemoglobin, i.e., oxyhemoglobin, carboxyhemoglobin, and deoxyhemoglobin. Serum albumin and hemoglobin are the primary constituents of blood plasma and red blood cells, respectively, and have been the subjects of extensive study. Hemoglobin also has distinct changes in its linear spectrum between ligated and nonligated states[56] that are expected to be reflected in THG.

2. THEORY

THG is the coherent conversion of light with frequency ω into light with frequency 3ω, i.e., wavelength $\lambda/3$, in a material that undergoes intense irradiation. It involves the absorption of three identical photons of energy $\hbar\omega$ and the emission of a single photon of energy $3\hbar\omega$ within the temporal uncertainty interval of $\omega^{-1} \sim 10^{-16}$ s. The resultant light propagates in the forward direction. A material's susceptibility to a given nonlinear conversion process is described by the susceptibility tensors, $\chi^{(n)}$, that relate the polarization field, denoted P, induced in the material to the electric field, denoted E, of the incident photon. Of the 81 independent elements included in the third-order nonlinear susceptibility tensor $\chi^{(3)}_{ijkl}(\omega_i, \omega_j, \omega_k, \omega_l)$, we are interested only in the terms associated with a uniformly polarized, single-frequency excitation field, i.e., $\omega_j = \omega_k = \omega_l$. This allows the fourth-rank tensor status of the susceptibility tensor to be suppressed and the THG polarization field $P^{(3)}(3\omega)$ to be expressed as

$$P^{(3)}(3\omega) = \chi^{(3)}(3\omega)E^3(\omega). \tag{1}$$

In a solution or other isotropic media, the measured value for $\chi^{(3)}(3\omega)$ is averaged over orientation and equal to $\frac{1}{3}[\chi^{(3)}_{xxxx}(3\omega) + \chi^{(3)}_{yyyy}(3\omega) + \chi^{(3)}_{zzzz}(3\omega)]$. The susceptibility $\chi^{(3)}(3\omega)$ is the term we seek to measure.

A. Resonant Enhancement

The underlying molecules that facilitate THG need not have real states available whose excitation energy corresponds to the incident photon energy or any multiple thereof. However, the THG process is resonantly enhanced if real energy levels are present at the fundamental (ω), second-harmonic (2ω), or third-harmonic (3ω) frequency. Thus the third-order susceptibility tensor may be dominated by either resonant or nonresonant mechanisms, which makes it convenient to write

$$\chi^{(3)}_{\text{Total}}(3\omega) \equiv \chi^{(3)}_{\text{nonresonant}}(3\omega) + \chi^{(3)}_{\text{resonant}}(3\omega). \tag{2}$$

Under the assumption that all molecules are in the electronic ground state prior to excitation, the resonance term generated in a perturbation expansion is[57]

$$\chi^{(3)}_{\text{resonant}}(3\omega) = \sum_{l,k,j} \frac{N\mu_{0l}\mu_{lk}\mu_{kj}\mu_{j0}}{\hbar^3(\omega_{l0} - 3\omega - i\gamma_{l0})(\omega_{k0} - 2\omega - i\gamma_{k0})(\omega_{j0} - \omega - i\gamma_{j0})}, \tag{3}$$

where N is the number of molecules and the indices refer to different electronic states, μ_{j0} is the electric dipole transition moment between the jth state and the ground state, γ_{j0} is the phenomenological damping coefficient that is inversely proportional to the decay rate from the jth state to the ground state, $\hbar\omega_{j0}$ is the energy difference between the jth state and the ground state, and the ω_{j0}, ω_{k0}, and ω_{l0} correspond to one-, two-, and three-photon resonances, respectively. The intermediate states are those closest to multiples of the incident photon energy, $\hbar\omega$, and the energies of the various states satisfy the relation $\hbar\omega_{l0} \geqslant \hbar\omega_{k0} \geqslant \hbar\omega_{j0}$. Resonance occurs as $\omega_{j0} \rightarrow \omega$, $\omega_{k0} \rightarrow 2\omega$, or $\omega_{l0} \rightarrow 3\omega$ and can significantly increase the magnitude of the susceptibility.[17,57] Implicit in this formalism is the notion that all photons in the excitation field have the same polarization, or parity, as well as energy.

1. One- and Three-Photon Resonances

The selection rules, based on conservation of parity, for enhancement by a single-photon resonance also apply to enhancement by a three-photon resonance. Thus the presence of peaks in the linear absorption spectrum of the solution, at frequencies ω and 3ω, is a good indication of whether such resonances are likely to be involved in THG [Eq. 3]. It is important to note that such resonant enhancement may be self-limiting in thick samples. When one- and three-photon resonances are strong, one- and

three-photon absorption by the material will deplete the incoming fundamental and outgoing third-harmonic waves, respectively.

2. Two-Photon Resonance

Two-photon absorption is an even-parity process, whereas, as above, linear absorption is an odd-parity process. Although parity selection rules are relaxed in noncentrosymmetric molecules, the two-photon resonant absorption remains difficult to predict on the basis of peaks in the linear absorption spectra at frequency 2ω. However, parity selection rules are expected to relax in larger molecules.[58] As two-photon absorption does not involve energy levels that have allowed single-photon transitions with the ground state, two-photon resonance can lead to enhancements of the susceptibility without a significant loss of optical power. Further, two-photon resonance is not likely to affect the index of refraction and thus the phase matching of a given nonlinear process.[17]

3. Nonresonant Contributions

In the case that the nonresonant component of $\chi^{(3)}(3\omega)$ is dominant, several semiempirical scaling laws have been proposed to account for the spectral dependence of $\chi^{(3)}(3\omega)$.[57,59–61] Miller's rule has been found to account for much of the spectral dependence of ionic crystals, for which

$$\chi^{(3)}_{\text{nonresonant}}(3\omega) \propto \chi^{(1)}(3\omega)[\chi^{(1)}(\omega)]^3 \propto [n^2(3\omega)-1] \times [n^2(\omega)-1]^3. \quad (4)$$

Wang's rule[60] has been found to account for much of the spectral dependence of gases, for which

$$\chi^{(3)}_{\text{nonresonant}}(3\omega) \propto [\chi^{(1)}(\omega)]^2 \propto [n^2(\omega)-1]^2. \quad (5)$$

Lastly, Boling's rule[62] includes local-field effects and should be more generally valid in the fluid phase, i.e.,

$$\chi^{(3)}_{\text{nonresonant}}(3\omega) \propto [n^2(\omega)+2]^2[n^2(\omega)-2]^2. \quad (6)$$

B. Microspectroscopy

The third-harmonic intensity that is generated from an axially symmetric material with susceptibility $\chi^{(3)}(3\omega)$ when irradiated by a tightly focused Gaussian beam, denoted $P(3\omega)$, is[10]

$$P(3\omega) = C(\omega)\left| b(\omega)\int_{-\infty}^{\infty} d\phi \exp(ib\Delta\kappa\phi)\frac{\chi^{(3)}(3\omega,\phi)}{(1+i2\phi)^2}\right|^2 P^3(\omega), \quad (7)$$

where $C(\omega)$ is a formulation of prefactors that depend on the geometry and efficiency of the collection system but are independent of the sample, $P(\omega)$ is the incident power, $b(\omega)$ is the confocal parameter, and the integration is over the normalized distance $\phi=z/b$ with the focus at $\phi=0$. In diffraction-limited geometries the confocal parameter is given by

$$b(\omega) = 2\pi n(\omega)\frac{w_o^2}{\lambda} = \frac{2n(\omega)\lambda}{\pi}\frac{[n^2(\omega)-\text{NA}^2]}{\text{NA}^2}, \quad (8)$$

where $n(\omega)$ is the index of refraction and w_o is the radius of the beam waist at the focal plane, expressed in terms of the numerical aperture (NA) of the objective. Lastly, the wave-vector mismatch between the excitation and the emitted third-harmonic fields, denoted, $\Delta\kappa$, is[57]

$$\Delta\kappa = 6\pi\frac{n(\omega)-n(3\omega)}{\lambda}. \quad (9)$$

Significant generation of THG in the far field occurs when the fundamental field can constructively drive the third-harmonic field and corresponds to small values of the product $b\Delta\kappa$. Under the present conditions of tight focusing, THG is near its maximal value for $b\Delta\kappa\sim 1$.

Since the elements of the nonlinear susceptibility are generally small in magnitude, e.g., $\chi^{(3)}(3\omega)\sim 10^{-14}$ esu for many solutions and $\chi^{(3)}(3\omega)\sim 10^{-17}$ esu for gases, THG signals from bulk samples tend to be small,[15,57] i.e., $P(3\omega)/P(\omega)\sim 10^{-8}$ for incident irradiance of $\sim 10^{10}$ W/cm^2. More significantly, in an isotropic medium, the Gouy phase shift encountered as a light wave traverses the focus causes the THG produced on one side of a focus to destructively interfere with THG produced on the other side and thus cancel the third-harmonic wave in the far-field.[63] However, the cancellation will be imperfect if the optical properties of the sample, i.e., the index of refraction and the nonlinear susceptibility, differ across the focal volume.[10,15] Tsang[16] and Barad *et al.*[10] have shown that the far-field third-harmonic intensity can be increased by many orders of magnitude when the focus spans an interface between two optically different materials. This renders THG microscopy particularly sensitive to optical interfaces and inhomogeneities on the spatial scale of the focal volume.[11,13,17–19]

It follows from Eq. (7) that the THG intensity from a Gaussian beam focused on a flat interface between two infinite homogeneous slabs of material is

$$P(3\omega)_{\text{Slab}_1/\text{Slab}_2} = C(\omega)\left|\chi^{(3)}_{\text{Slab}_1} b_{\text{Slab}_1}\mathcal{J}(b_{\text{Slab}_1}\Delta\kappa_{\text{Slab}_1}) - \chi^{(3)}_{\text{Slab}_2} b_{\text{Slab}_2}\mathcal{J}(b_{\text{Slab}_2}\Delta\kappa_{\text{Slab}_2})\right|^2 P^3(\omega), \quad (10)$$

where we have neglected reflection and absorption and make use of the dimensionless phase-matching integral, $\mathcal{J}(b\Delta\kappa)$, defined as

$$\mathcal{J}(b\Delta\kappa) \equiv \int_0^{\infty} d\phi \frac{\exp(ib\Delta\kappa\phi)}{(1+i2\phi)^2}. \quad (11)$$

An absolute measurement of $\chi^{(3)}(3\omega)$ is complicated by the need to determine the factors in $C(\omega)$.[64,65] Yet a relative value of $\chi^{(3)}(3\omega)$ is often of sufficient utility. In particular, the value of $\chi^{(3)}(3\omega)$ for a solution is measured relative to the glass substrate, typically fused silica, that forms the sample container.[15,52,54,66] One implements this paradigm by collecting third-harmonic light both from the interface between the sample solution and the glass, with intensity $P(3\omega)_{\text{solution/glass}}$, and from the interface between the glass and the air, with intensity $P(3\omega)_{\text{glass/air}}$. It follows from Eq. (10) that the ratio of these measurements is

$$\frac{P(3\omega)_{\text{solution/glass}}}{P(3\omega)_{\text{glass/air}}} = \left[\frac{\chi^{(3)}_{\text{glass}}(3\omega) b_{\text{glass}}(\omega) J(b_{\text{glass}}\Delta\kappa_{\text{glass}}) - \chi^{(3)}_{\text{solution}}(3\omega) b_{\text{solution}}(\omega) J(b_{\text{solution}}\Delta\kappa_{\text{solution}})}{\chi^{(3)}_{\text{glass}}(3\omega) b_{\text{glass}}(\omega) J(b_{\text{glass}}\Delta\kappa_{\text{glass}}) - \chi^{(3)}_{\text{air}}(3\omega) b_{\text{air}}(\omega) J(b_{\text{air}}\Delta\kappa_{\text{air}})} \right]^2. \quad (12)$$

Noting that $\chi^{(3)}_{\text{air}}(3\omega) \sim 0$, this becomes

$$\frac{P(3\omega)_{\text{solution/glass}}}{P(3\omega)_{\text{glass/air}}} \cong \left[1 - \frac{\chi^{(3)}_{\text{solution}}(3\omega) b_{\text{solution}}(\omega) J(b_{\text{solution}}\Delta\kappa_{\text{solution}})}{\chi^{(3)}_{\text{glass}}(3\omega) b_{\text{glass}}(\omega) J(b_{\text{glass}}\Delta\kappa_{\text{glass}})} \right]^2. \quad (13)$$

Solving for the susceptibilities leads to

$$\frac{\chi^{(3)}_{\text{solution}}(3\omega)}{\chi^{(3)}_{\text{glass}}(3\omega)} = \frac{J(b_{\text{glass}}\Delta\kappa_{\text{glass}}) b_{\text{glass}}(\omega)}{J(b_{\text{solution}}\Delta\kappa_{\text{solution}}) b_{\text{solution}}(\omega)} \times \left\{ 1 \pm \left[\frac{P(3\omega)_{\text{solution/glass}}}{P(3\omega)_{\text{glass/air}}} \right]^{1/2} \right\}. \quad (14)$$

The resolution of the sign ambiguity requires additional information that is either gathered through consideration of resonances or, as will be discussed in Section 4, obtained by comparative measurements. The general validity of this approach was examined by Barille *et al.*,[52] who demonstrated remarkable consistency between their femtosecond measurements at an excitation wavelength of 1.5 μm and previous picosecond measurements[52,53,67] at an excitation wavelength of 1.9 μm.

In the case of a solution composed of a solute and a solvent, the different components may contribute to Eq. (14) with opposite signs. The correct value of the susceptibility ratio of the hydrated solute, defined as $\chi^{(3)}_{\text{solute}}(3\omega)/\chi^{(3)}_{\text{glass}}(3\omega)$, may be determined from the measured power ratio of the solution, denoted $P(3\omega)_{\text{solution/glass}}/P(3\omega)_{\text{glass/air}}$, given knowledge of both the power ratio and the susceptibility ratio of the solvent, i.e., $P(3\omega)_{\text{solvent/glass}}/P(3\omega)_{\text{glass/air}}$ and $\chi^{(3)}_{\text{solvent}}(3\omega)/\chi^{(3)}_{\text{glass}}(3\omega)$, respectively. In the case in which the solute and solvent occur with solvated volume fractions of v and $1-v$, respectively, the measured power ratio of the dissolved solute is

$$\frac{\chi^{(3)}_{\text{solute}}(3\omega)}{\chi^{(3)}_{\text{glass}}(3\omega)} = \frac{J(b_{\text{glass}}\Delta\kappa_{\text{glass}}) b_{\text{glass}}(\omega)}{J(b_{\text{solution}}\Delta\kappa_{\text{solution}}) b_{\text{solution}}(\omega)} \times \left(1 + \frac{1}{v} \left\{ \pm \left[\frac{P(3\omega)_{\text{solution/glass}}}{P(3\omega)_{\text{glass/air}}} \right]^{1/2} - (1-v) \times \left[\frac{P(3\omega)_{\text{solvent/glass}}}{P(3\omega)_{\text{glass/air}}} \right]^{1/2} \right\} \right). \quad (15)$$

Note that the sign of the solvent term has been taken to be negative (Section 4) and the confocal parameter, index and dispersion of the dissolved solute are correctly taken to be the same as the solution, as these are properties of the bulk. The remaining sign ambiguity must be resolved independently.

3. METHODS

A. Imaging

Our imaging apparatus consists of a laser scanning microscope[68] with the collection of transmitted light for THG imaging and epi-emitted light for simultaneous two-photon-excited fluorescence laser scanning microscopy (Fig. 1). The excitation source for imaging was a locally constructed 1.054 μm Nd:glass oscillator with an 80 MHz repetition rate and ~100 fs duration pulses. We used a 40×0.65 NA Zeiss excitation objective ($f=4$ mm) and a fused-silica collection lens ($f=6$ mm). The detectors were Hamamatsu R6357 photomultipliers (PMTs) with quartz windows that were connected to a resistive load and amplified. Colored glass filters (Corning UG-11) were used to block all but the third-harmonic light from reaching the PMT tube. For two-photon-excited fluorescence, bandpass (550 ± 25 nm) and colored glass filters (Corning BG-39) were used to block extraneous light.

B. Microspectroscopy

1. Apparatus and Materials

Spectroscopic measurements were performed without the use of the x–y scan mirrors (Fig. 1). The excitation source was a Ti:sapphire oscillator (Mira 900-F with a 10 W Verdi pump, Coherent, Inc., Santa Clara, California) with a 76 MHz repetition rate and ~100 fs duration; this

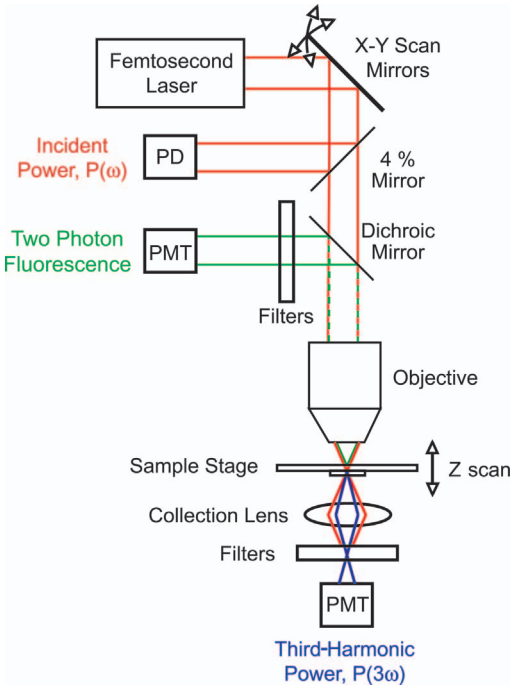

Fig. 1. Multiphoton imaging and THG spectroscopy apparatus. Images were collected using a 1.054 μm, 100 fs Nd:glass pulsed laser. Spectroscopic measurements were made using a Ti:sapphire laser with 100 fs pulses and wavelengths between 760 and 1000 nm. PD, photodiode; PMT, photomultiplier tube.

source was tuned over a wavelength range of 760 to 1000 nm. We used 40×0.65 and 0.75 NA Zeiss excitation objectives. The detector was a Hamamatsu R6353 PMT with quartz windows that was connected to a resistive load and amplified. As with imaging, colored glass filters (Corning UG-11) were used to block all but the third-harmonic light from reaching the PMT tube. For fundamental wavelengths below 810 nm, the colored glass filters were supplemented with a 265 nm bandpass filter.

Our sample containers were microcuvettes (3520; Vitrocom, Mountain Lakes, New Jersey) with flat 200 μm thick glass walls (Duran 8340) and a 500 μm wide chamber to hold the solution. The Duran 8340 glass has optical properties similar to those of fused silica (Appendix B).

Our samples consisted of deionized water, neat benzene (BX0212-6; Omni Solv, Charlotte, North Carolina), and aqueous solutions of 1 mM Rhodamine B chloride (R-6626; Sigma-Aldrich, St. Louis, Missouri), 0.5 mM solution of Fura-2 pentasodium salt (F-6799; Molecular Probes, Eugene, Oregon) with 3.3 mM ethylene glycol bis(β-aminoethyl ether)-N,N,N′,N′ tetra-acetic acid (EDTA) (E-478; Fisher Scientific, Pittsburgh, Pennsylvania), 0.5 mM Cascade-Blue trisodium salt (C-687; Molecular Probes), 0.75 mM BSA (81-066-1; Miles Scientific, Naperville, Illinois), and hemoglobin. The hemoglobin solutions are at physiological concentrations 2 mM ($\sim$17 g/dL) and represent three different ligand-binding states. These include a 98% (v/v) oxyhemoglobin (HbO_2) solution (300881R0; Instrumentation Laboratories, Lexington, Massachusetts), a mixed 60% (v/v) carboxylated and 40% (v/v) oxygenated carboxyhemoglobin (HbCO) solution (300879R0; Instrumentation Laboratories), and a deoxygenated (Hb) solution (>80% based on spectroscopic measurements) that was formed by bubbling N_2 through the oxyhemoglobin solution.

2. THG Measurement

We seek to derive the third-order susceptibility ratio of our solution relative to glass, $\chi^{(3)}_{\text{solution}}(3\omega)/\chi^{(3)}_{\text{glass}}(3\omega)$, by measuring the ratio of THG power from the solution/glass and glass/air interfaces, i.e., $P(3\omega)_{\text{solution}}/P(3\omega)_{\text{glass/air}}$. Measurements were made in a manner similar to the method employed by Barille *et al.*[52] We scanned through the solution-filled microcuvette along the propagation axis of the incident beam and collected third-harmonic light from both the solution/glass and the glass/air interfaces [Fig. 2(A)]. The third-harmonic power, $P(3\omega)$, traces out two bell-shaped profiles as the focus is swept across the two interfaces [Fig. 2(B)]. The peak of the profile centered on the lower solution/glass interface corresponds to $P(3\omega)_{\text{solution/glass}}$, and the peak of the profile centered on the bottom of the glass side corresponds to $P(3\omega)_{\text{glass/air}}$ [Fig. 2(B)]. The half-widths at half-maximum of each profile indicates the extent of the confocal parameter [Eq. (8)].[10] The THG signal was averaged over $\sim$20 such sweeps. The maximum incident irradiance at the sample was $\sim10^{10}$ W/cm^2, and the maximum THG efficiency was $P(3\omega)/P(\omega)\sim5\times10^{-7}$.

The measurement of peak third-harmonic power was repeated at different incident powers to form graphs of $P_{\text{solution/glass}}(3\omega)$ and $P_{\text{glass/air}}(3\omega)$ versus the incident power $P(\omega)$ [Fig. 2(C)]. The relation between the two measured third-harmonic powers was fit as a cubic function of incident power, i.e., $P_{\text{solution/glass}}(3\omega)=\alpha_{\text{solution/glass}}P^3(\omega)+P_{\text{dark}}$ and $P_{\text{glass/air}}(3\omega)=\alpha_{\text{glass/air}}P^3(\omega)+P_{\text{dark}}$, where $\alpha_{\text{solution/glass}}$, $\alpha_{\text{glass/air}}$, and P_{dark} are the fit coefficients. The parameter P_{dark} was fit to the two interfaces simultaneously and corrected for dark noise in the PMT. This procedure, as opposed to a measurement of THG at a single

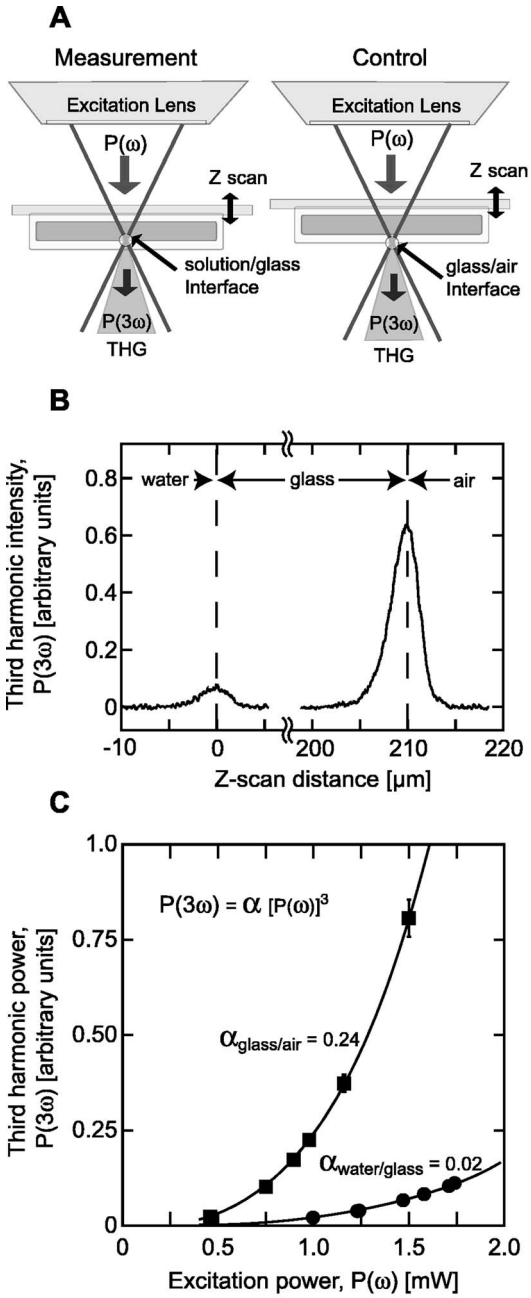

Fig. 2. Third-harmonic spectroscopic measurement procedure applied to deionized water. (A) Close-up of the sample and apparatus. Third-harmonic generated light is collected from both the sample/vessel interface and the vessel/air interface, and their ratio is used to infer sample properties. (B) A THG signal is generated as an interface is scanned through the focus of the beam. The peak of the THG intensity profile is measured for different incident laser powers. The half-width at half-maximum is proportional to the confocal parameter b. (C) The THG intensities from both the sample/vessel interface and the vessel/air interface demonstrate the anticipated cubic dependence on laser power.

incident power, increases the signal-to-noise ratio of our measurement. It further minimizes potentially confounding effects that have noncubic scaling with the incident power, such as excited-state absorption and the nonlinear refraction.[59]

C. Data Reduction

Prior to additional corrections, the ratio of third-harmonic powers is given by $R_{\mathrm{THG}}(\omega)=\alpha_{\mathrm{solution/glass}}(\omega)/\alpha_{\mathrm{giass/air}}(\omega)$. This ratio must be corrected for reflection at interfaces and linear absorption by the glass cuvette.

1. Linear Absorption

Linear absorption and transmission spectra, between 250 and 1000 nm, of all model solutions were obtained with a Cary 50 (Varian, Palo Alto, California) spectrophotometer. Those for the different ligation states of hemoglobin are taken from published measurements[56] [Fig. 7(A)]. The near-infrared absorption spectra of water was further culled from the literature.[69] Duran glass measurements are from the manufacturer's literature (Vitrocom) and corrected to account for reflection at normal incidence by using the Fresnel equation for the reflectivity, $r(\omega)$, i.e.,

$$r(\omega)_{\mathrm{SiO_2/solution}}=\frac{n_{\mathrm{glass}}(\omega)-n_{\mathrm{solution}}(\omega)}{n_{\mathrm{solution}}(\omega)+n_{\mathrm{glass}}(\omega)}, \tag{16}$$

and measurements for benzene [Fig. 10(B)] are a composite of data taken over wavelengths that ranged from 0.78 to 1.25 μm[70] and 1.33 to 1.8 μm.[71]

2. Reflection Coefficients

To account for the different third-harmonic and fundamental powers transmitted through each interface, we calculated the reflection coefficients $r(\omega)$ and $r(3\omega)$ by using the Fresnel equation [Eq. (16)]. The absorptivity $a(\omega)$ of the glass substrate was extracted from linear transmission measurements, $t(\omega)$, with use of the calculated reflection coefficients, $r(\omega)$, and the formula $a(\omega)=\{[1-r(\omega)]^2-t(\omega)\}/[1-r(\omega)]^2$.

3. Linear Dispersion

Calculation of the reflection coefficients, $r(\omega)$, the diffraction-limited confocal parameter, $b(\omega)$ [Eq. (8)], and the wave-vector mismatch, $\Delta\kappa(\omega)$ [expression (9)], depends on prior knowledge of the dispersion of the linear refractive index, $n(\omega)$. Unfortunately, precise refractive index measurements and models do not exist for many materials. This is especially notable at wavelengths shorter than 400 nm, which are important in estimations of $\Delta\kappa(\omega)$ and $r(3\omega)$. The uncertainty in $\Delta\kappa(\omega)$ is graphically illustrated in the case of benzene [Fig. 3(A)], where we plot the results from two dispersion models for benzene (Appendix A), each of which fits all available dispersion data equally well at visible wavelengths but which significantly diverges for ultraviolet wavelengths.

4. Confocal Parameter

The confocal parameter, $b(\omega)$, can be measured directly from the axial extent of the THG profile [Fig. 2(B)][10] as noted above. In diffraction-limited geometries, where the linear dispersion of the sample is known, the confocal parameter can be calculated with Eq. (8). We use both approaches and note that diffraction-limited THG measurements can simultaneously be used as a means to independently measure the linear index through this correspondence. Typical confocal parameters for this experiment were between 5 and 7 μm.

5. Volume Fractions

Calculation of the susceptibility ratio [Eq. (15)] for the case of solutions requires an estimate of the hydrated volume fraction of the solute under study. The volume of the hydrated complex is relevant because the electronic interaction between solute and solvent is integral to the solution's nonlinear optical properties.[49,50,73–75] Thus we are essentially interested in measuring the susceptibility of the solvated complex.

As a means to estimate the hydrodynamic volume of Rhodamine B in water, and thus the volume fraction of solvated Rhodamine B chloride in a 1 mM aqueous solution, we make use of the rotational relaxation time of Rhodamine B in solution[74] and approaches based on functional groups.[76,77] We note that close to 50% (w/v) of the Rhodamine B may be dimerized at a concentration of 1 mM.[78,79] We use this estimate for Rhodamine B and the

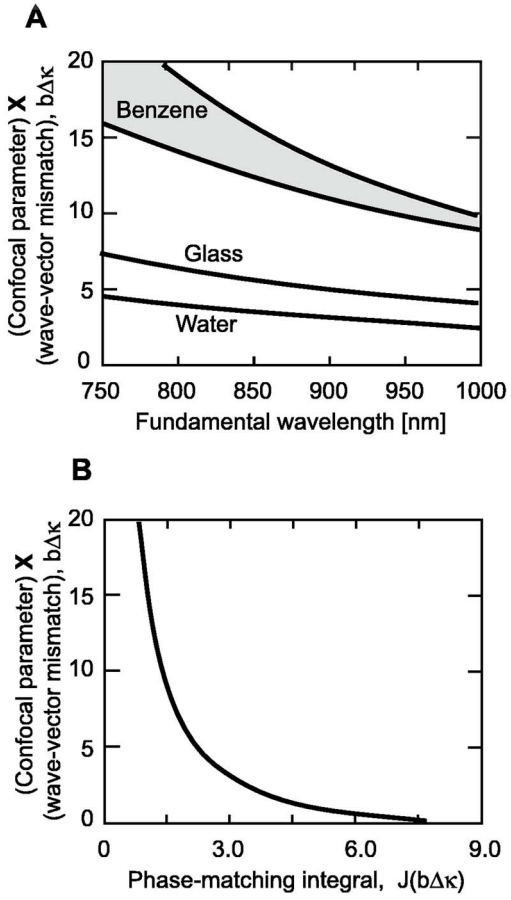

Fig. 3. (A) Theoretical curves of the confocal parameter times the wave-vector mismatch, $b\Delta\kappa$. Curves are calculated from linear dispersion models for water, benzene, and Duran glass in the case of diffraction-limited geometry. The band representing benzene is bounded by the curves predicted by two different models of dispersion.[32,72] (B) The phase-matching integral,[25] $J(b\Delta\kappa)$.

ratios of volume estimates from functional group-based approaches[76,77] to calculate the hydrated volume fraction of Fura-2 dye in a 0.5 mM aqueous solution. Literature measurements also contribute to our volume fraction estimates of BSA and hemoglobin solutions.[80,81]

6. Corrected Ratio of THG Power

The corrected, fitted ratio of THG power is

$$R_{\mathrm{THG}}(\omega) \equiv \frac{\alpha_{\mathrm{solution/glass}}(\omega)}{\alpha_{\mathrm{glass/air}}(\omega)} \times \frac{[1-r^2(\omega)_{\mathrm{glass/solution}}]^3[1-a(\omega)_{\mathrm{glass}}]^3}{[1-r^2(3\omega)_{\mathrm{glass/solution}}][1-a(3\omega)_{\mathrm{glass}}]}. \tag{17}$$

This measure controls for linear absorption, reflections, and some of the intercapillary and intersample variation and mitigates drift in laser parameters and sample orientation. The susceptibility ratio for solvents [Eq. (14)] is re-expressed as

$$\frac{\chi^{(3)}_{\mathrm{solution}}(\omega)}{\chi^{(3)}_{\mathrm{glass}}(\omega)} = \frac{J(b_{\mathrm{glass}}\Delta\kappa_{\mathrm{glass}})b_{\mathrm{glass}}(\omega)}{J(b_{\mathrm{solotion}}\Delta\kappa_{\mathrm{solution}})b_{\mathrm{solution}}(\omega)} \times[\beta(\omega)\rho(\omega) \pm \sqrt{R_{\mathrm{THG}}(\omega)}], \tag{18}$$

where the coefficient

$$\beta(\omega) \equiv \frac{J(b_{\mathrm{glass/solution}}\Delta\kappa_{\mathrm{glass}})b_{\mathrm{glass/solution}}(\omega)}{J(b_{\mathrm{glass/air}}\Delta\kappa_{\mathrm{glass}})b_{\mathrm{glass/air}}(\omega)} \tag{19}$$

accounts for the possibility of changes in the confocal parameter of the glass at the two interfaces due to aberrations and the coefficient

$$\rho(\omega) = \left\{\frac{[1-r^2(\omega)_{\mathrm{glass/solution}}]^3}{[1-r^2(3\omega)_{\mathrm{glass/solution}}]}\right\}^{1/2} \tag{20}$$

accounts for reflections at the interfaces of the cuvette. The former term is typically unity but in some experiments was found to be close to 0.8 while the latter term is greater than 0.9. The phase integral $J(b\Delta\kappa)$ [Eq. (11)] can be numerically evaluated[25,52] as a function of the product $b\Delta\kappa$ [Fig. 3(B)]. Lastly, for the case of a solution, the corrected susceptibility expression [Eq. (15)] is

$$\frac{\chi^{(3)}_{\mathrm{solute}}(\omega)}{\chi^{(3)}_{\mathrm{glass}}(\omega)} = \frac{J(b_{\mathrm{glass}}\Delta\kappa_{\mathrm{glass}})b_{\mathrm{glass}}(\omega)}{J(b_{\mathrm{solution}}\Delta\kappa_{\mathrm{solution}})b_{\mathrm{solution}}(\omega)}\left\{\beta(\omega)\rho(\omega) + \frac{1}{v}\left[\pm\sqrt{R_{\underset{\mathrm{solvent}}{\mathrm{THG}}}(\omega)} - (1-v)\sqrt{R_{\underset{\mathrm{solvent}}{\mathrm{THG}}}(\omega)}\right]\right\}, \tag{21}$$

with $\beta(\omega)$ and $\rho(\omega)$ given above [Eqs. (19) and (20)].

4. EXPERIMENTAL RESULTS

We consider first the image formation characteristics of THG solely as motivation for our spectroscopic studies. We then consider a systematic study of model solutions, i.e., water, benzene, Rhodamine B, Fura-2, and BSA solutions, followed by different function states of hemoglobin in solution, i.e., oxy-, carboxy-, and deoxyhemoglobin solutions. In all cases, the above theoretical framework is used to interpret our measurements of THG intensity, $P(3\omega)$, in terms of the third-order nonlinear susceptibility $\chi^{(3)}(3\omega)$.

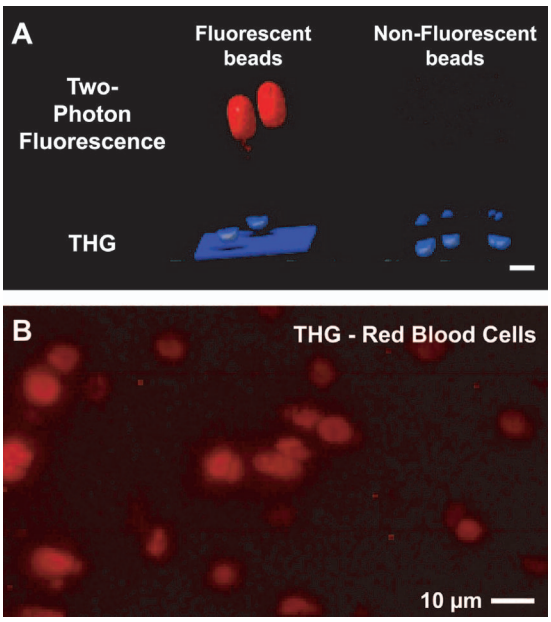

Fig. 4. Two-photon-excited fluorescence and THG imaging. (A) A comparison of two-photon-excited fluorescence and THG images. Unlike two-photon-excited fluorescence, THG can be collected from both fluorescent and nonfluorescent beads. THG can be seen to be primarily produced at interfaces perpendicular to the excitation beam, including the coverslip beneath the fluorescent samples. In this case a shadow of the beads is cast on the coverslip due to the distortion of the excitation beam. (B) Third-harmonic image showing the high contrast of red blood cells in solution without the use of dyes.

A. THG Imaging

The enhancement of THG at an interface is illustrated through a comparison of two-photon-excited fluorescence and THG imaging of 10 μm diameter fluorescein-labeled microspheres versus equally sized unlabeled glass beads that sit in a drop of water on a glass coverslip [Fig. 4(A)]. The microspheres are readily resolved in entirety with two-photon fluorescence, while only the interfaces normal to the incident beam, at either the microsphere/water or the water/glass interface, yield third-harmonic light [Fig. 4(A)]. The elongation of images for either modality is a consequence of the difference in axial resolution (z_o = 5.0 μm) compared with lateral resolution (r_o = 1.0 μm). The top surfaces of the beads appear dark as a result of the absorption of the third-harmonic light by the fluorescent beads. The shadowing on the glass surface results from distortion of the excitation beam as it passes through the bead. Critically, there is no fluorescent signal for the case of imaging glass beads, yet THG at the water/glass interface leads to an image of the top and bottom surfaces of the beads [Fig. 4(A)].

As motivation for our studies on the THG by hemoglobin, we applied THG imaging to human red blood cells in solution without the use of dyes. A maximal projection

through a 5 μm stack of unprocessed images leads to the well-known view of red blood cells as concave disks [Fig. 4(B)].

B. Microspectroscopy

We now turn to quantitative spectroscopy of model compounds and hemoglobin in solution. We report our measurements in terms of the corrected and fitted ratio of third-harmonic power at the solution/glass interface relative to that at the glass/air interface [Eq. (17)]. These are used, when appropriate, to derive the corresponding ratio of susceptibilities [Eqs. (18) and (19)]. A discussion of the uncertainty in all terms is presented toward the end of this subsection.

1. Model Solvents

Measurements of THG at the water/glass interface relative to the glass/air interface show that $R_{\mathrm{THG}}(\omega)$, the ratio of third-harmonic powers [Eq. (17)], decreased as a monotonic function of wavelength [Fig. 5(A)]. We resolve the sign ambiguity in the susceptibility ratio $\chi^{(3)}_{\mathrm{H_2O}}(3\omega)/\chi^{(3)}_{\mathrm{glass}}$ [Eqs. (18)–(20)] by considering the spectral trend in $R_{\mathrm{THG}}(\omega)$ to be related to a one-photon resonance near a wavelength of 970 nm [Fig. 5(A′)]. The errors bars in Figs. 5(A) and 5(A′) capture an ~11% uncertainty in the measurement of $R_{\mathrm{THG}}(\omega)$, whereas the additional systematic uncertainty in $\chi^{(3)}_{\mathrm{H_2O}}(3\omega)/\chi^{(3)}_{\mathrm{glass}}$ is expected to be less than 4%.

The third-harmonic spectrum of benzene is essentially constant over the range of measured wavelengths [Figs. 5(B) and 5(B′)], consistent with an absence of one- and two-photon resonances over the range of our measurements. The third-harmonic spectrum does not reflect the long wavelength tail of the ultraviolet absorption band in benzene that, in principle, could contribute to a three-photon resonance; this suggests that the dominant contribution to $\chi^{(3)}(3\omega)$ of benzene is nonresonant. The sign ambiguity in the estimate of $\chi^{(3)}_{\mathrm{benzene}}(3\omega)/\chi^{(3)}_{\mathrm{glass}}$ [Eqs. (18) and (19)] is resolved to be positive on the basis of two consid-

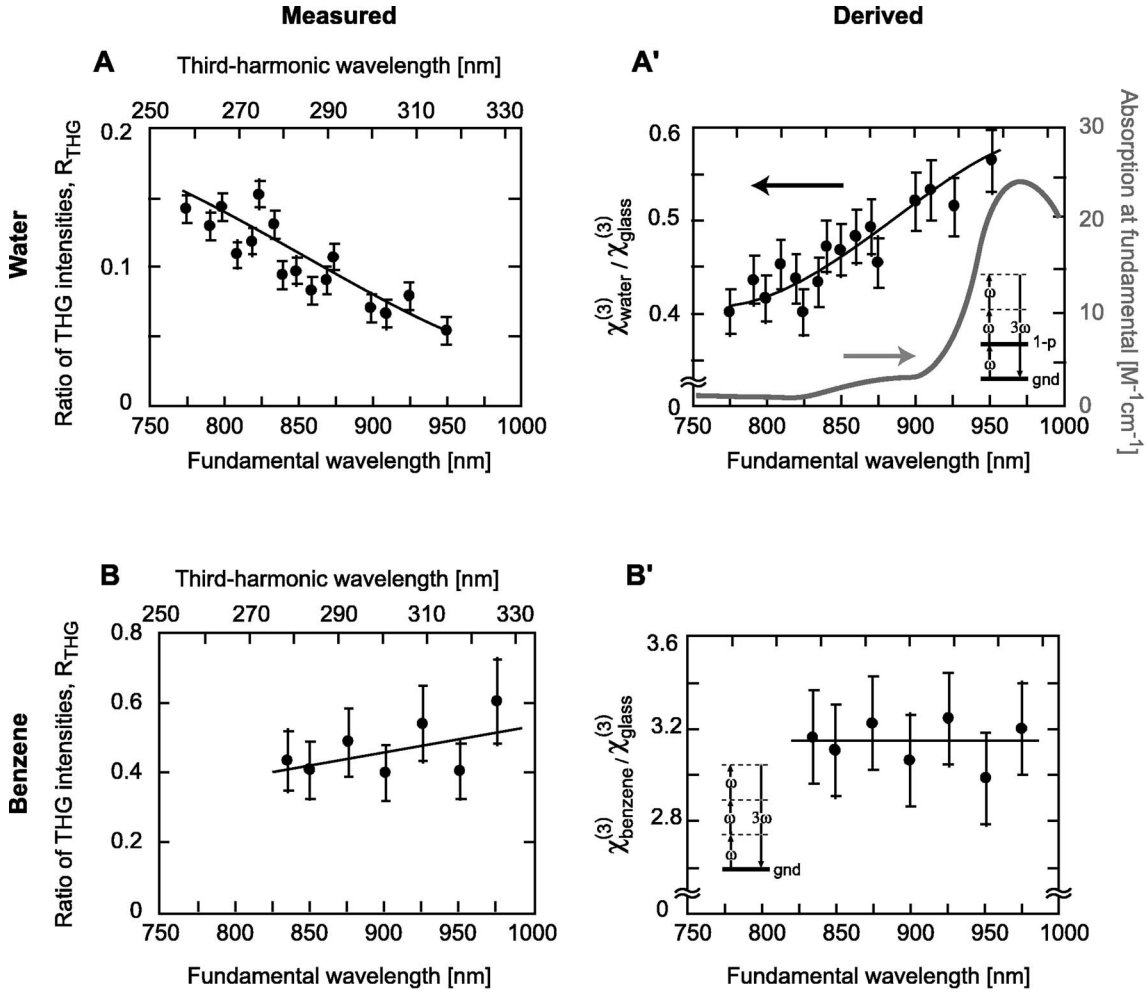

Fig. 5. Third-harmonic spectra of water and benzene; each datum is the mean ± standard error (±SE). Linear absorption spectra between 250 to 1000 nm were obtained with a Cary 50 spectrophotometer. (A) The third-harmonic intensity ratio, $R_{\mathrm{THG}}(\omega)$, of deionized water. The term $R_{\mathrm{THG}}(\omega)$ is the ratio of the cubic-fit coefficients of the sample/vessel interface to that of the vessel/air interface and is related to the ratio of the third-order susceptibility ratio by Eq. (18). (A′). We show the derived third-order susceptibility ratio of water and glass, $\chi^{(3)}_{\mathrm{H_2O}}(3\omega)/\chi^{(3)}_{\mathrm{glass}}$ (black arrow and left scale), and the linear absorption of water at the fundamental wavelength (gray arrow and right scale). The correspondence between the THG and the linear absorption spectrum indicates a one-photon resonant enhancement; see inset energy diagram (B) The third-harmonic intensity ratio, $R_{\mathrm{THG}}(\omega)$, of neat benzene. (B′) The calculated third-order susceptibility ratio of benzene and glass is relatively constant, suggesting that the dominant contribution to $\chi^{(3)}(3\omega)$ of benzene is nonresonant.

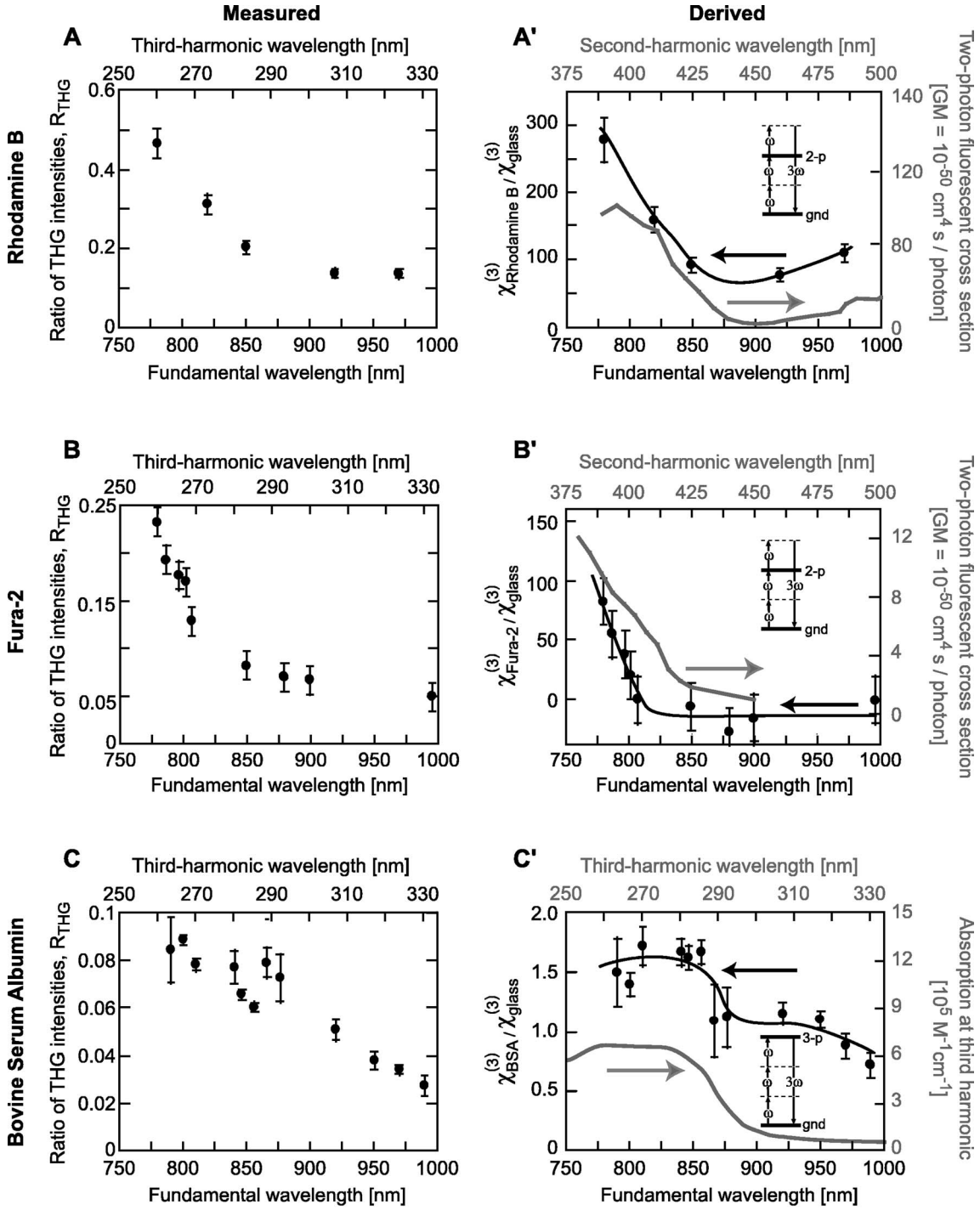

Fig. 6. Third-harmonic spectrum of Rhodamine B, Fura-2, and BSA; each datum is the mean ±SE. (A) We show the third-harmonic intensity ratio, $R_{THG}(\omega)$, of an aqueous solution of 1 mM Rhodamine B. (A′) We show the derived third-order susceptibility ratio of Rhodamine B, $\chi^{(3)}_{Rhodamine}(3\omega)/\chi^{(3)}_{glass}$, and the two-photon action cross section.[84] The correspondence between the THG and two-photon action indicates a strong two-photon resonant enhancement in Rhodamine B below 850 nm. (B) The third-harmonic intensity ratio, $R_{THG}(\omega)$, of an aqueous solution of 0.5 mM Fura-2. (B′) The third-order susceptibility ratio of Fura-2, $\chi^{(3)}_{Fura\text{-}2}(3\omega)/\chi^{(3)}_{glass}$, and the two-photon action cross section[85–87] track each other, indicating a two-photon resonant enhancement. (C) The third-harmonic intensity ratio, $R_{THG}(\omega)$, of a 0.75 mM solution of BSA. (C′) The calculated third-order susceptibility ratio of BSA and glass, $\chi^{(3)}_{BSA}(3\omega)/\chi^{(3)}_{glass}$ suggests that $\chi^{(3)}(3\omega)$ for BSA has a three-photon resonant enhancement from 750 to 850 nm. We display the linear absorption of BSA over the region relevant to three-photon resonance.

erations. First, the hyperpolarizabilities associated with double bonds between carbon atoms in benzene are anticipated to lead to much larger $\chi^{(3)}(3\omega)$ values for this molecule than for distilled water.[51,82,83] Second, a choice of the negative root in Eq. (14) leads to comparable values for $\chi^{(3)}(3\omega)$ in water and benzene over the range of 875 to 950 nm. The systematic uncertainty in the susceptibility ratio of benzene is ~17%.

2. Aqueous Solutions

The third-harmonic spectrum of a 1 mM solution of Rhodamine B chloride shows a sharp decrease with increasing wavelength, with a break in the slope near 850 nm [Figs. 6(A) and 6(A′)]. The sign ambiguity in the estimate of $\chi^{(3)}_{\text{Rhodamine}}(3\omega)/\chi^{(3)}_{\text{glass}}$ [Eqs. (19)–(21)] is easily resolved if we assume that the susceptibility of the Rhodamine B solution is greater than that of pure water. We use Eqs. (21) through (18) to find $\chi^{(3)}_{\text{Rhodamine}}(3\omega)/\chi^{(3)}_{\text{glass}}$ and note that it mirrors the two-photon-excited fluorescent cross-section measurements[84] in Rhodamine B; this suggests the presence of a strong two-photon resonance [Fig. 6(A′)]. The systematic error introduced into $\chi^{(3)}_{\text{Rhodamine}}(3\omega)/\chi^{(3)}_{\text{glass}}$ by our estimate of volume fraction, $v=0.0004$, is ~50% [Eq. (15)].

The third-harmonic spectrum of a solution of 0.5 mM Fura-2 pentasodium salt and 3.3 mM EGTA shows a sharp decrease with increasing wavelength with a break in the slope at a wavelength of 800 nm [Fig. 5(C)]. Unlike the case of Rhodamine B, the $R_{\text{THG}}(\omega)$ solvent background is a 3.3 mM EGTA solution (data not shown). We resolve the sign ambiguity in the estimate of $\chi^{(3)}_{\text{Fura-2}}(3\omega)/\chi^{(3)}_{\text{glass}}$ [Eq. (21)] by assuming that the susceptibility of the dye solution is greater than that of water alone. Our estimate of the volume fraction of the hydrated Fura-2 complex at ~0.07% introduces an ~70% systematic error in our derived value of $\chi^{(3)}_{\text{Fura-2}}(3\omega)/\chi^{(3)}_{\text{glass}}$. The susceptibility ratio, $\chi^{(3)}_{\text{Fura-2}}(3\omega)/\chi^{(3)}_{\text{glass}}$ shows a spectral profile similar to the measured[85–87] two-photon-excited fluorescent cross section of Fura-2 [Fig. 6(B′)]. This suggests a strong two-photon resonance.

The THG spectrum of a 0.75 mM solution of BSA also shows a decrease with increasing wavelength [Fig. 6(C)]. The sign ambiguity in the estimate of $\chi^{(3)}_{\text{BSA}}(3\omega)/\chi^{(3)}_{\text{glass}}$ [Eq. (21)] is resolved if we assume that the susceptibility of the albumin is enhanced by a three-photon resonance in the linear absorption spectrum of albumin [Fig. 6(C′)]. Dispersion and volume fraction uncertainties result in a less than 12% systematic uncertainty in our value for $\chi^{(3)}_{\text{BSA}}(3\omega)/\chi^{(3)}_{\text{glass}}$.

3. Hemoglobin Solutions

The linear absorption spectrum of hemoglobin shows a prominent Soret absorption band that peaks near a wavelength of 420 nm [Fig. 7(*A*); central gray]. The corresponding dip in the measured value of $R_{\text{THG}}(\omega)$ of these solutions (Fig. 8) is highly suggestive of a two-photon resonance. We use this correspondence to resolve the sign ambiguity in Eq. (21). We use the refractive index estimate of oxyhemoglobin [Fig. 7(B); see Appendix A for derivation] to estimate the wave-vector mismatch [expression (9)]. We estimate that the volume fraction of hemoglobin in a 2 mM solution to be ~12% for the various hemoglobin solutions[80,81] and estimate that this introduces a systematic error of ~6.5% in our susceptibility ratios $\chi^{(3)}_{\text{O}_2\text{–Hb}}(3\omega)/\chi^{(3)}_{\text{glass}}$. An unaccounted-for feature at long wavelengths may reflect the additional involvement of a three-photon resonance [left-hand gray band in Fig. 7(A)] or the solvent.

4. Uncertainty

The standard deviation of the measured peak THG power was between 1.5% and 5.5% of the peak value across the wavelength range of 760 to 1000 nm, with the exact percentage dependent on the incident power, the interface, and the sample. The uncertainties in the cubic fits of the peak THG power led to uncertainties as high as 6% in the value of $R_{\text{THG}}(\omega)$ [Eq. (17)] within the same session. Measurements of the same substance on different days could lead to variations as large as 13% in the values of $R_{\text{THG}}(\omega)$. The experimental errors are represented as standard errors (SEs) of the mean in the graphs of $R_{\text{THG}}(\omega)$ and $\chi^{(3)}_{\text{solution}}(3\omega)/\chi^{(3)}_{\text{glass}}$ (Figs. 5, 6, and 8). They result from an average over two to five estimates of $R_{\text{THG}}(\omega)$; we recall that each estimate involves the ratio of cubic equation fits through six to ten data points for both solution/glass and glass/air interfaces [Fig. 2(C)]. The SE are of the same order as uncertainties in absolute measurements of the susceptibility in glass.[65]

Additional, systematic uncertainties in the susceptibility ratios (Tables 1 and 2) result from the propagation of uncertainty in the dispersion of relevant materials. The dipersion of Duran 8340 glass [Eq. (A1)], benzene[72] [Eqs.

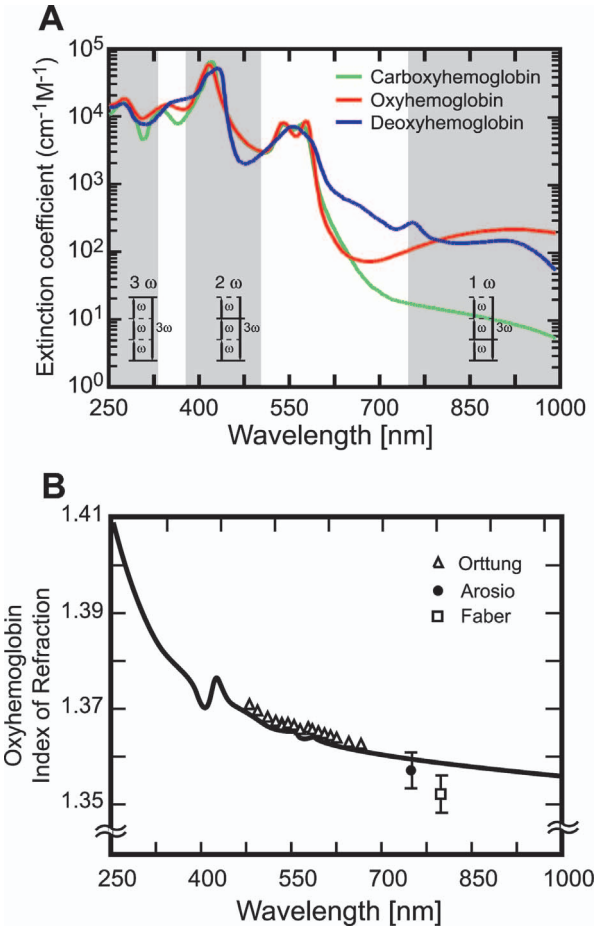

Fig. 7. (A) Linear absorption spectrum of oxy-, deoxy-, and carboxyhemoglobin.[56] The wavelength bands corresponding to potential one-photon, two-photon, and three-photon resonances are highlighted and labeled. (B) The estimated refractive index of oxyhemoglobin (Appendix A) and point index measurements taken by Orttung and Warner[88] (500 to 650 nm), Arosio *et al.*[81] (750 nm) and Faber *et al.*[89] (800 nm).

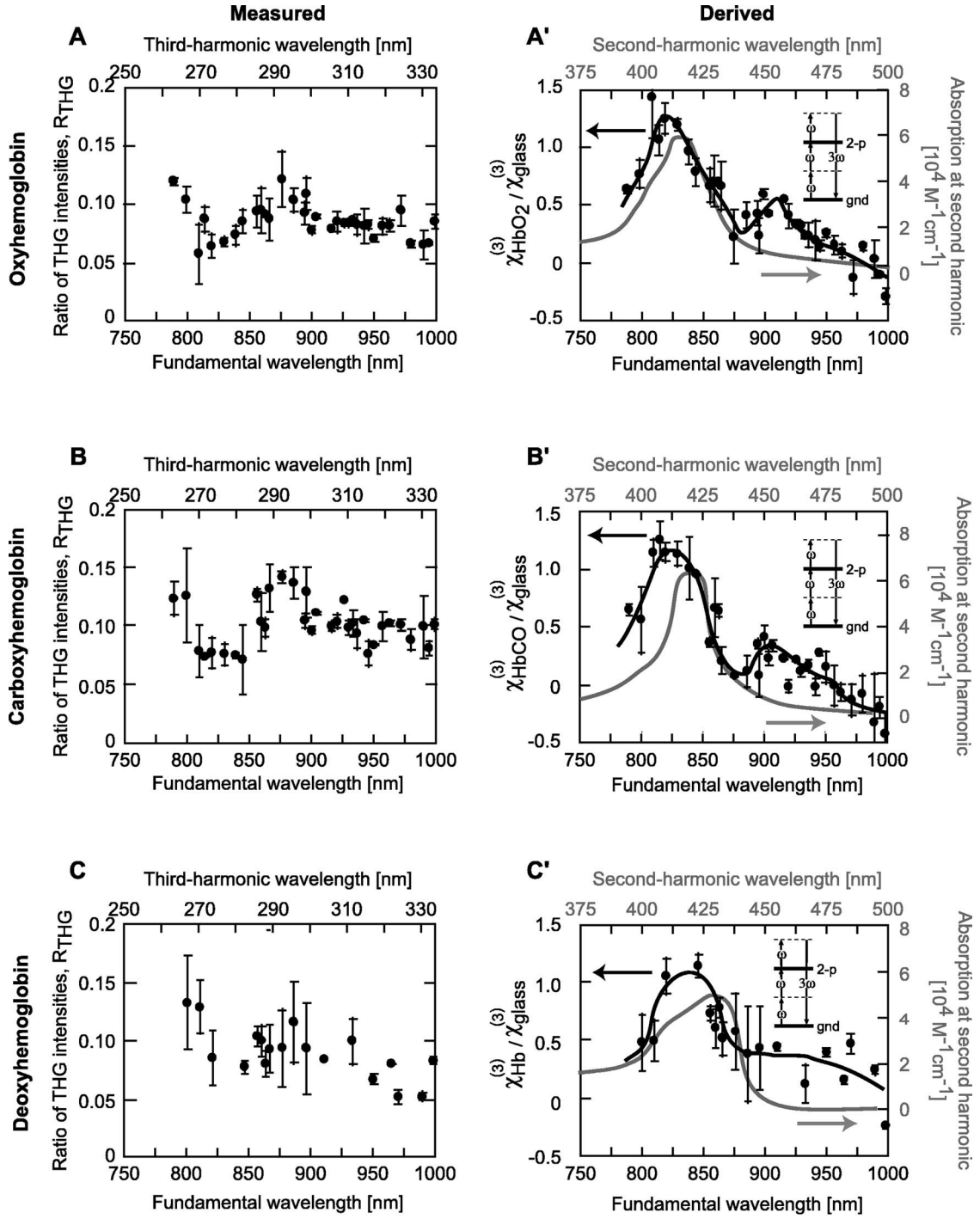

Fig. 8. Third-harmonic spectrum of oxy-, carboxy-, and deoxyhemoglobin solutions (this work) together with linear absorption measurements;[56] each datum is the mean ±SE. (A) The third-harmonic intensity ratio, $R_{\mathrm{THG}}(\omega)$, of a 2 mM oxyhemoglobin solution. (A′) The correspondence between the derived third-order susceptibility ratio of oxyhemoglobin, $\chi^{(3)}_{\mathrm{HbO_2}}(3\omega)/\chi^{(3)}_{\mathrm{glass}}$, and the linear absorption from 375 to 500 nm indicates a two-photon resonant enhancement. (B) We show the third-harmonic intensity ratio, $R_{\mathrm{THG}}(\omega)$, of a 2 mM, 60% (v/v) carboxylated hemoglobin solution. (B′) The derived third-order susceptibility ratio of 60% (v/v) carboxyhemoglobin, $\chi^{(3)}_{\mathrm{HbCO}}(3\omega)/\chi^{(3)}_{\mathrm{glass}}$, and the linear absorption in the two-photon resonance range suggest a two-photon resonant enhancement. (C) The third-harmonic intensity ratio, $R_{\mathrm{THG}}(\omega)$, of a 2 mM, ~95% (v/v) deoxygenated hemoglobin solution. (C′) The calculated third-order susceptibility ratio of deoxyhemoglobin and glass, $\chi^{(3)}_{\mathrm{Hb}}(3\omega)/\chi^{(3)}_{\mathrm{glass}}$, and the linear absorption of deoxyhemoglobin in the two-photon absorption regime.

(A2) and (A3)], water[91] [Eq. (A4)], BSA [Eq. (A5)], Rhodamine B, Fura-2, and hemoglobin [Fig. 7(B)] is approximated by numerical formulas (Appendix A). The uncertainty in the values of the susceptibility ratio introduced by these approximations is maximal at the blue side of the spectrum, where there are few published measurements of the refractive index to constrain models (Appendix A). At an excitation wavelength of 750 nm, we es-

Table 1. Dispersion Estimates and Uncertainties at λ=250 and 750 nm

Material	$n(3\omega)$	$\frac{\delta n(3\omega)}{n(3\omega)}$ (%)	$n(\omega)$	$\frac{\delta n(\omega)}{n(\omega)}$ (%)	Uncertainty in $\frac{\chi^{(3)}_{\text{solute}}(3\omega)}{\chi^{(3)}_{\text{glass}}(3\omega)}$ (%)
Duran glass[a]	1.530	<0.2	1.469	<0.1	<3
Benzene[72]	1.610	1.7	1.480	0.4	17
Water[90]	1.379	<0.01	1.329	<0.001	<1
Dyes[90]	1.384	2	1.332	1	30
BSA[a]	1.390	<1	1.337	<0.5	<5
Hemoglobin[a]	1.410	<1	1.360	<0.05	<5
	λ=250 nm	λ=250 nm	λ=750 nm	λ=750 nm	λ=750 nm

[a]Appendix A.

Table 2. Volume Fraction Estimates and Uncertainties of Solutes in Solution

Solute	Hydrodynamic Radius (nm)	Concentration (mM)	Volume Fraction, υ (%)	Uncertainty in υ (%)	Uncertainty in $\frac{\chi^{(3)}_{\text{solute}}(3\omega)}{\chi^{(3)}_{\text{glass}}(3\omega)}$ (%)
Rhodamine B[74,77]	0.5	1.0	0.04	45	50
Fura-2[74,77]	0.7	0.5	0.07	50	70
BSA[80,81]	3.14	0.75	7	20	7.5
Hemoglobin[80,81]	2.96	2.0	12	11	6.5

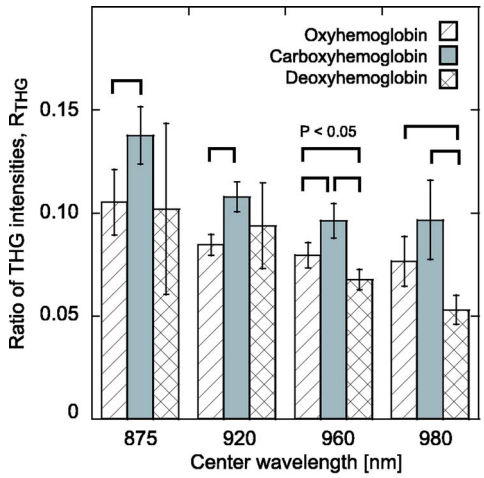

Fig. 9. (Color online) Third-harmonic intensity ratio of hemoglobin in different oxidation states averaged over 20 nm bands. Error bars represent two SE; significance at the 95% confidence level is indicated by a bar.

timate that the uncertainty in $\chi^{(3)}_{\text{solution}}(3\omega)/\chi^{(3)}_{\text{glass}}(3\omega)$ that results from uncertainty in the linear dispersion is <3%, ~17%, <1%, <5%, and <5% for Duran 8340, benzene, water, BSA, and hemoglobin, respectively (Table 1).

A second source of uncertainty in the susceptibility ratios concerns the volume of solution [Eqs. (15) and (21)] occupied by the solvated form of Rhodamine B, Fura-2, BSA, and hemoglobin in 1, 0.5, 0.75, and 2 mM solutions that is estimated to be 0.04%, 0.07%, 7%, and 12%, respectively. Uncertainties in the volume fraction estimates dominate the systematic uncertainty in the derived susceptibility ratios for these solutions (Table 2). This large uncertainty in values gleaned from the literature is due in part to the presence of a substrate where adsorption may play a role.[73,92–96]

5. Spectral Discrimination of Hemoglobin Ligand States

The final issue concerns the ability to discriminate among the three ligation states of hemoglobin on the basis of their relative THG spectra, $R_{\text{THG}}(\omega)$. In principle, this can be accomplished wherever the spectra do not intercept. However, for the signal-to-noise ratios achieved in our measurements, we could distinguish among all three states (95% confidence level) in a 20 nm wide band only near a center wavelength of 960 nm (Fig. 9). At other center wavelengths, two of the three possible states could be distinguished (Fig. 9).

5. DISCUSSION

We confirm that far-field THG is significantly enhanced when the focal volume is bisected by an optical interface[11,13,17–19] (Fig. 4). We use this phenomenon to investigate the nonlinear spectra of solutions over the wavelength range of 750 to 1000 nm by collecting THG from the interface of sample solutions and their glass containers[52,54] (Fig. 2). The susceptibility ratio of pure solutions, $\chi^{(3)}_{\text{solution}}(3\omega)/\chi^{(3)}_{\text{glass}}$ [Eq. (16)], is inferred from power-dependent measurements of the THG from the solution/glass and glass/air interfaces.[11,52,54] This calculation requires sample-specific models of linear dispersion [Fig. 7(B)], which we generate and collate in Appendix A. We further derive the susceptibility ratios of hydrated solutes, $\chi^{(3)}_{\text{solute}}(3\omega)/\chi^{(3)}_{\text{glass}}$, from THG measurements on solutions, by subtracting the THG due to the solvent from the

total THG from the solution [Eqs. (15) and (21)]. Miller's rule [expression (4)] indicates that the nonlinear susceptibility, $\chi^{(3)}_{\text{glass}}$, of the glass substrate is approximately constant over the 750 to 1000 nm range of wavelengths, which implies that spectral features in the susceptibility ratio $\chi^{(3)}_{\text{sample}}(3\omega)/\chi^{(3)}_{\text{glass}}$ reflect features in the susceptibility, $\chi^{(3)}_{\text{sample}}(3\omega)$, of the sample (Appendix B).

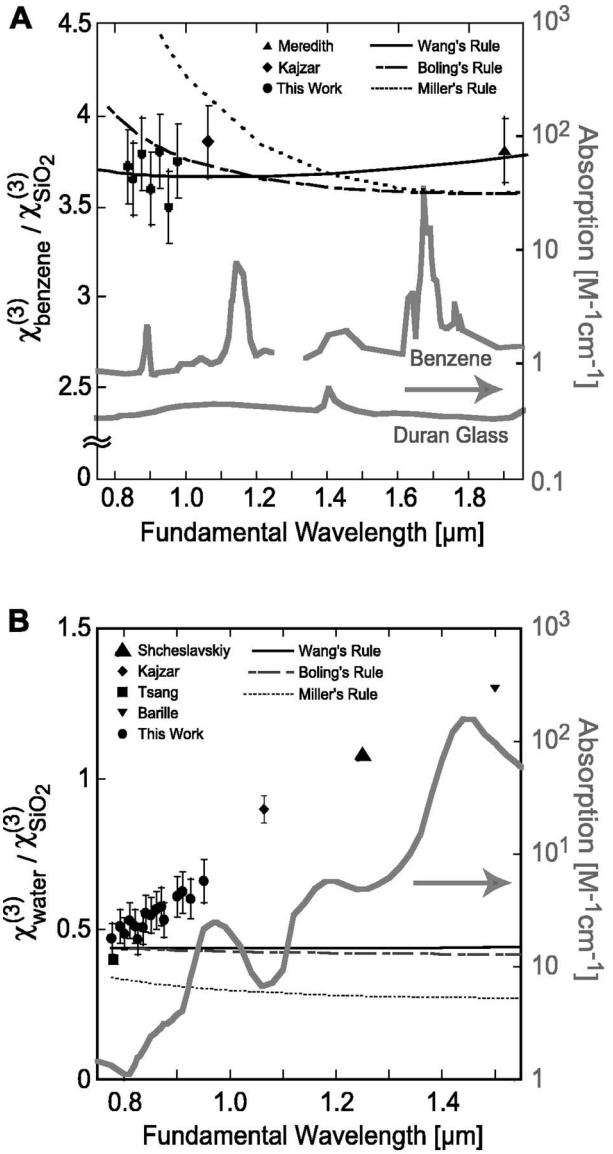

Fig. 10. Comparison of THG and linear absorption spectra with semiempirical rules and linear absorption spectra. The data from THG measurements made here have been shifted by the ratio of Miller's rules for Duran glass and SiO_2 in order to compare them with values reported in the literature (this factor is ~1.17, Appendix B). (A) Benzene: the THG measurement at 1.06 μm used 13 ns pulses and a Maker fringe technique,[66] and the 1.9 μm measurement used ~30 ns pulses and a triple-wedge technique.[53,67] Linear absorption measurements in benzene are piecewise composed from measurements over wavelengths of 0.78 to 1.25 μm[70] and 1.33 and 1.8 μm.[71] Linear absorption values for the Duran glass are based on transmission measurements and are corrected to account for reflection using the Fresnel equations [Eq. (15)]. (B) Water: the THG measurement at 780 nm used 100 fs pulses and a variant of the Maker fringe approach,[16] those at 1.25 and 1.5 μm used 40 to 130 fs pulses and an experimental protocol similar to that used here,[52,54] and the measurement at 1.06 μm used 13 ns pulses and a Maker fringe technique.[66] Linear absorption measurements are due to Segelstein.[69]

To evaluate the accuracy of our spectroscopic approach in pure solutions, we compare our measured values of the nonlinear susceptibility ratio of deionized water and benzene with measurements in the literature[52,54,55,66,67] (Fig. 10). Most literature measurements are made relative to fused silica (SiO_2), so an accurate comparison with our results requires that we first scale our results by the ratio of the susceptibility of our Duran glass to that of SiO_2. This scaling factor is achieved by our applying Miller's rule [expression (4)] and indicates that the glass/SiO_2 susceptibility ratio is ~1.17 (Appendix B).

The scaled values of $\chi^{(3)}_{\text{sample}}(3\omega)/\chi^{(3)}_{SiO_2}$ for benzene and water found here (Fig. 10) are in good correspondence with those measured at different wavelengths and with different approaches. Literature values are plotted with the measurements made here, and error bars are included whenever they are available. Systematic errors in our values are not accounted for in the figure (Tables 1 and 2). The close agreement among measurements made with pulse widths ranging from 30 ns to 40 fs supports the understanding of THG as a purely electronic effect, not unduly modulated by the nonlinear index of refraction or short-time-scale solvation processes.[97–100]

The microspectroscopy approach[52,54,101] adopted here relies on tightly focused ~100 fs pulse-width, ~1 nJ laser pulses to sample ~50 μm^3 volumes of solution. It can be performed with exactly the same pulse shape,[102–104] energy, and duration used in laser scanning nonlinear imaging. Previous spectroscopic studies based on the Maker fringe technique relied on softly focused ~1 mJ laser pulses, 10 ns or longer, to sample much larger volumes.[39,53,66,105] Whereas the Maker fringe technique yields third-harmonic phase information, which is discarded in the present technique, both approaches appear to have similar experimental errors.

We also compare the various semiempirical rules for calculating $\chi^{(3)}(3\omega)$ values [expressions (4)–(6)] with those found here and in the literature for the cases of benzene and water (Fig. 10). These formulations are not expected to perform well in solutions or near resonance. However, Wang's rule[60] [expression (5)] and, to a lesser extent, Boling's rule[59,62] [expression (6)] predict the relatively flat spectrum of benzene [Fig.10(A)], which may indicate a broader utility for use with nonresonant solutions.

A. Nonlinear Spectra

Comparisons between linear and nonlinear spectra show common features and demonstrate one-, two-, and three-photon resonances in THG spectra that correspond to linear absorption features at the fundamental, second, and third harmonics of the excitation beam as well as two-photon absorption resonances. We find evidence of a one-photon resonance in the $\chi^{(3)}(3\omega)$ spectra of water [Figs. 5 (A′) and 10(B)]; a two-photon resonance in the $\chi^{(3)}(3\omega)$ of Rhodamine B, Fura-2, and hemoglobin [Figs. 6(A′), 6(B′), and 7(A)]; a three-photon resonance in the $\chi^{(3)}(3\omega)$ of BSA [Fig. 6(C′)]; and no resonance in benzene [Fig. 5(B)]. The two-photon resonances in the Rhodamine B and Fura-2

spectra are identified by comparison with two-photon-excited fluorescence cross-section spectra [Figs. 6(A′) and 6(B′)] and confirm that THG may be used as a probe of two-photon excited states that are not accessible with linear absorption measurements.[87]

The degree of modulation in $\chi^{(3)}(3\omega)$ associated with a resonant enhancement varies dramatically between compounds. For example, Fura-2 shows a greater than 20-fold increase in $\chi^{(3)}(3\omega)$ associated with a 10-to-10^2-times increase in its two-photon action cross section, whereas Rhodamine B shows an ~3-fold increase in $\chi^{(3)}(3\omega)$ associated with an $\sim 10^2$-fold increase in the two-photon cross section (Fig. 6′). These differences follow, in part, from the variable contribution of nonresonant terms to the susceptibility [Eq. (2)]. For example, the magnitude of the susceptibility ratio of nonresonant benzene $[\chi^{(3)}_{\text{benzene}}(3\omega)/\chi^{(3)}_{\text{glass}} \cong 3.2]$ is about twice as large as that of the resonance peaks of water, BSA, and hemoglobin, and, of the materials reviewed here, only Fura-2's peak resonant value equals the nonresonant value of Rhodamine B $[\chi^{(3)}_{\text{Rhodamine}}(3\omega)/\chi^{(3)}_{\text{glass}} \cong 77]$. Thus the resonant modulation $\chi^{(3)}_{\text{resonant}}/\chi^{(3)}_{\text{nonresonant}}(3\omega)$ in the susceptibility spectrum is most appreciable for compounds such as oxyhemoglobin and Fura-2, where the nonresonant value is relatively low.

B. Potential Application to Imaging

The ratio of THG powers, $R_{\text{THG}}(\omega)$, represents image luminosity as collected in a THG microscope. $R_{\text{THG}}(\omega)$ is not directly proportional to the nonlinear susceptibility [Eq. (18)]; as a result, resonance enhancements may appear as an increase or a decrease in THG luminosity [Figs. 5(A), 5(A′), and 6)]. Nonetheless, $R_{\text{THG}}(\omega)$ spectra can be used to distinguish different solutions. We also find that at physiological concentrations (~2 mM), hemoglobin solutions consisting of 98% (v/v) oxyhemoglobin, 60% (v/v) carboxyhemoglobin and 40% (v/v) oxyhemoglobin (corresponding with heavy smoke inhalation), or 90% (v/v) deoxyhemoglobin show significant differences in their $R_{\text{THG}}(\omega)$ spectra when averaged over 20 nm spectral bands (Fig. 9).

Additional factors are needed to enhance the signal-to-noise ratio before THG can be used to determine the oxidation state of hemoglobin in flowing red blood cells. Possibly, THG from red blood cells may provide a higher contrast than the hemoglobin solution/glass interface,[91,106] though such measurements would require a tight focus so as to minimize the orientation effects of the cell. It is also possible that successive single-power measurements might be more useful for discriminating between oxidation states. Acquisition of repeated measurements at the same power has the advantage allowing rapid comparisons across cells while surrendering the potential to extract accurate absolute values for the third-order susceptibility. Finally, the ability to distinguish among oxidation states of hemoglobin in red blood cells depends only on the ratio of THG at different excitation wavelengths and does not require corrections for linear absorption and refraction of the incident and THG light.

The two-photon absorption resonance in the THG spectrum of hemoglobin [Figs. 8(A′), 8(B′), and 8(C′)] does not lead to a significantly larger value for the nonlinear susceptibility than the value found for BSA [Fig. 6(C′)]. This suggests that damage induced under nonlinear excitation will not be preferentially driven in either compound. In capillaries, whose ~5 μm diameter is of the order of two confocal parameters, the observed two-photon resonance implies that 820 nm is an optical wavelength for the visualization of flowing red blood cells against fluorescently labeled plasma.[107,108] Conversely, irradiating a sample at 880 nm may be best to minimize photodamage to hemoglobin.

The large two-photon resonance in the Rhodamine B and Fura-2 indicates that common fluorescent dyes used for two-photon microscopy may have a latent information channel available in THG. In all cases the THG channel will preferentially probe dyes in the vicinity of interfaces, effectively creating a complementary contrast mechanism.

APPENDIX A

We discuss the derivation and application of the phenomenological formulas used to calculate the refractive indices of silicone dioxide, Duran 8340 glass, benzene, water, and solutions of Rhodamine B, Fura-2, BSA, and hemoglobin.

1. SiO_2 and Duran Glass

The dispersion of SiO_2 is fit by a well-known formula,[109] whereas that for Duran 8340 glass is approximated by this dispersion equation to fit reported index values in the visible range.[110] We have

$$n_{\text{SiO}_2 \text{ or Duran}}(\lambda) = \left[1 + \frac{n_1}{1 - \left(\frac{\lambda_1}{\lambda}\right)^2} + \frac{n_2}{1 - \left(\frac{\lambda_2}{\lambda}\right)^2} + \frac{n_3}{1 - \left(\frac{\lambda_3}{\lambda}\right)^2} \right]^{1/2}, \tag{A1}$$

where the common parameters are $n_1 = 0.897479$, $\lambda_1 = 3145.816$ nm, $n_2 = 0.4079426$, and $\lambda_2 = 340.9419$ nm. For SiO_2, $n_3 = 0.6961663$ and $\lambda_3 = 261.5422$ nm; for Duran glass, $n_4 = 0.7376285665$ and $\lambda_4 = 279.6276303$ nm.

2. Benzene

Significant differences in the value of $\Delta\kappa$ arise when one compares refractive index models for benzene constructed in the visible wavelength[32,72] [Fig. 2(A)]. Comparison of the model calculation with existing refractive index measurements does not allow for a clear choice between models.[111] We use the average index of the two models. The first is[72]

$$n_{\text{benzene}}(\lambda) = n_0 \left[1 + \left(\frac{\lambda_0}{\lambda}\right)^2 \right], \tag{A2}$$

with $n_0 = 1.21501$ and $\lambda_0 = 76.56803$ nm, and the second is[32]

$$n_{\text{benzene}}(\lambda) = n_0\left[1 + \frac{n_1}{1 - \left(\frac{\lambda_1}{\lambda}\right)^2}\right]^{1/2}, \quad \text{(A3)}$$

with $n_0 = 1.205$, $n_1 = 0.501$, and $\lambda_1 = 170$ nm.

3. Water

Models of the refractive index, $n(\omega)$ of water, as in the case of benzene, exhibit significant divergence at wavelengths in the ultraviolet part of the spectrum.[32,112] Our choice of models[90] is dictated by favorable comparison with reported measurements across the full range of wavelengths, 250 to 750 nm. We use[112]

$$n_{\text{water}}(\lambda, S, T) = n_0 + (n_1 + n_2 T + n_3 T^2)S - n_4 T^2 + \frac{n_5 + n_6 S + n_7 T}{\lambda} - \left(\frac{n_8}{\lambda}\right)^2 + \left(\frac{n_9}{\lambda}\right)^3, \quad \text{(A4)}$$

where S is salinity in parts per thousand, T is temperature in Celsius, λ is in nanometers, and the parameter values are $n_0 = 1.31405$, $n_1 = 1.779 \times 10^{-4}$, $n_2 = -1.05 \times 10^{-6}$, $n_3 = 1.60 \times 10^{-6}$, $n_4 = 2.02 \times 10^{-6}$, $n_5 = 15.868$, $n_6 = 1.155 \times 10^{-2}$, $n_7 = -4.23 \times 10^{-2}$, $n_8 = 66.20$, and $n_9 = 103.681$.

4. Dye Solutions

We approximate the wavelength dependence of the index of the dye solutions by scaling the dispersion curve of saltwater[90] [Eq. (A4)] to match an existing measurement[113] of the concentration-dependent index increment, $dn(\omega)/dc$, of Rhodamine B solutions at a wavelength of 780 nm. This gives an effective salinity of 2% (v/v) ($S = 20$) for 1 mM solutions of Rhodamine B; the same index increment was used for a 0.5 mM solution of Fura-2.

5. Bovine Serum Albumin

We use existing measurements of $dn(\omega)/dc$ at various wavelengths[114–116] (see Table 3) to construct a concentration-dependent dispersion increment model for BSA:

$$\frac{dn_{\text{BSA}}(\lambda)}{dc} = -\frac{\lambda}{118} + 162 + \frac{15\,000}{\lambda} + \left(\frac{0.056}{\lambda}\right)^2, \quad \text{(A5)}$$

where λ is in nanometers.

6. Hemoglobin

We estimate the dispersion of oxyhemoglobin solutions with a Taylor expansion of the Kramers–Kronig integral that relates the real and imaginary components of the complex refractive index[89] $n_c(\omega) = n(\omega) + in'(\omega)$. The imaginary component of the refractive index is related to the molar absorption coefficient $\epsilon(\omega)$ by[117]

$$n'(\omega) = c\,\ln(10)\frac{\epsilon(\omega)}{2\omega}, \quad \text{(A6)}$$

where c is the speed of light and $\omega = 2\pi c/\lambda$. We approximate the local dispersion features of oxyhemoglobin by fitting the $n'(\omega)$ absorption spectra in the 250–1000 nm wavelength range, with r Gaussians representing r absorption bands, such that $n'(\omega)$ can be expressed as the sum

$$n'(\omega) = \sum_r A_r \exp\left[\frac{(\Omega_r - \omega)^2}{2\sigma_r^2}\right], \quad \text{(A7)}$$

where $\sigma_r(\omega) \equiv (\Omega_r - \omega_{1/2})/\sqrt{2\ln(2)}$, Ω_r is the resonance angular frequency, $\omega_{1/2}$ is the frequency at half of the peak height, and A_r is the maximum value of $n'(\omega)$ for the r'th absorption band. Variations in the index due to local absorption bands can then be expressed as[118]

$$\Delta n(\omega) = \sqrt{2}\sum_r \frac{A_r}{\sigma_r}(\Omega_r - \omega)\exp\left[\frac{(\Omega_r - \omega)^2}{2\sigma_r^2}\right]. \quad \text{(A8)}$$

The results of this approach are then scaled and provided with a linear offset to fit existing measurements of $dn(\omega)/dc$ in oxyhemoglobin over the 450–800 nm wavelength range[88,89] [Table 4; Fig. 7(B)].

APPENDIX B

Schott's Duran 8340 glass, also designated as Corning 7740 Pyrex, is a borosilicate glass (81% SiO_2, 13% B_2O_3, and 4% AlO_3) with similar optical properties ($n\nu = 1.474$ and Abbe number of 65.7) to pure fused SiO_2 ($n\nu = 1.458$ and Abbe number of 67.8).[110] Boron is added primarily to reduce the melting temperature and is not thought to change the nonlinear properties of the glass.[119] Nonetheless, according to Miller's rule [expression (4)], the third-order susceptibility of the Duran glass is 17.9% to 17.2% larger than the value of $\chi^{(3)}(3\omega)$ for fused SiO_2 over the 750–1000 nm wavelength range. Measurements of $\chi^{(3)}(3\omega)$ in glasses of different indices support the magnitude of this estimate,[119–121] although the difference in $\chi^{(3)}(3\omega)$ values[59,61] may be as large as 100%. Miller's rule

Table 3. Linear Dispersion Increment of Bovine Serum Albumin

Wavelength	436 nm	488 nm	546 nm	578 nm	1060 nm
$dn(\omega)/dc$	0.1924 ml/g	0.192 ml/g	0.1854 ml/g	0.1901 ml/g	0.181 ml/g
Reference	116	115	116	114	115

Table 4. Linear Dispersion Increment of Oxyhemoglobin

Wavelength	500 nm	650 nm	750 nm	800 nm
$dn(\omega)/dc$	0.198 ml/g	0.1900 ml/g	0.170 ± 0.01 ml/g	0.143 ± 0.02 ml/g
Reference	88	88	81	89

also indicates that the value of $\chi^{(3)}(3\omega)$ for either glass will smoothly decrease by about 10% over the same range of wavelengths. This has been generally supported by measurements in fused SiO_2 and borosilicate glass at wavelengths ranging from 1.064 to 2.1 μm, which show a less than 20% change (with 7% to 15% variation) in the value $\chi^{(3)}(3\omega)$ for a given glass.[59,65]

ACKNOWLEDGMENTS

We thank Zvi Kam for the gift of a quartz lens and Earl Dolnick for assistance with the electronics. Financial support was provided by the National Science Foundation, Integrative Graduate Education and Research Traineeship program (G. O. Clay); the Burroughs Welcome–funded La Jolla Interfaces in Science (A. C. Millard and C. B. Schaffer); the David and Lucille Packard Foundation (D. Kleinfeld); the National Institutes of Health (NIH), National Center for Research Resources (D. Kleinfeld and J. S. Squier); and the NIH, National Institute of Biomedical Imaging and Bioengineering (D. Kleinfeld and J. A. Squier).

Corresponding author D. Kleinfeld may be reached at the Department of Physics 0374, University of California, 9500 Gilman Drive, La Jolla, California 92093, or by e-mail at dk@physics.ucsd.edu.

*Present address, Center for Biomedical Imaging Technology, University of Connecticut Health Center, Farmington, Connecticut 06030.

†Present address, Department of Biomedical Engineering, Cornell University, Ithaca, New York 14853.

‡Present address, Spectra-Physics, Inc., Mountain View, California 94039.

**Present address, Department of Physics, Colorado School of Mines, Golden, Colorado 80401.

REFERENCES

1. W. R. Zipfel, R. M. Williams, and W. W. Webb, "Nonlinear magic: multiphoton microscopy in the biosciences," Nat. Biotechnol. **21**, 1369–1377 (2003).
2. W. Denk, "Two-photon scanning photochemical microscopy: mapping ligand-gated ion channel distributions," Proc. Natl. Acad. Sci. U.S.A. **91**, 6629–6633 (1994).
3. W. Denk and K. Svoboda, "Photon upmanship: why multiphoton imaging is more than a gimmick," Neuron **18**, 351–357 (1997).
4. W. Denk, J. H. Strickler, and W. W. Webb, "Two-photon laser scanning fluorescence microscopy," Science **248**, 73–76 (1990).
5. P. J. Campanola, D. W. Young, A. E. Cowan, C. Roychoudhuri, and L. M. Loew, "Applications in nonlinear optical microscopy," Commun. Dis. Public Health4, 191–192 (1997).
6. D. L. Wokosin, V. E. Centonze, S. Crittenden, and J. White, "Three-photon excitation fluorescence imaging of biological specimens using an all-solid-state laser," Bioimaging **4**, 1–7 (1996).
7. I. Graczynski, H. Malak, and J. R. Lakowicz, "Multi-photon excitation of DNA stains DAPI and Hoechst," Bioimaging **4**, 138–148 (1996).
8. S. W. Hell, K. Bahlmann, M. Schrader, A. Soini, H. Malak, I. Grycznyski, and J. R. Lakowicz, "Three-photon excitation in fluorescence microscopy," J. Biomed. Opt. **1**, 71–74 (1996).
9. S. Maiti, J. B. Shear, R. M. Williams, W. R. Zipfel, and W. W. Webb, "Measuring serotonin distribution in live cells with three-photon excitation," Science **275**, 530–532 (1997).
10. Y. Barad, H. Eisenberg, M. Horowitz, and Y. Silberberg, "Nonlinear scanning laser microscopy by third harmonic generation," Appl. Phys. Lett. **70**, 922–924 (1997).
11. J. Squier, M. Muller, G. J. Brakenhoff, and K. Wilson, "Third harmonic generation microscopy," Opt. Express **3**, 315–321 (1998).
12. D. Oron, D. Yelin, E. Tal, S. Raz, R. Fachima, and Y. Silberberg, "Depth-resolved structural imaging by third-harmonic generation microscopy," J. Struct. Biol. **147**, 3–11 (2004).
13. D. Yelin and Y. Silberberg, "Laser scanning third-harmonic-generation microscopy in biology," Opt. Express **5**, 169–175 (1999).
14. D. Yelin, D. Oron, E. Korkotian, M. Segal, and Y. Silberberg, "Third-harmonic microscopy with a titanium-sapphire laser," Appl. Phys. B **74**, 97–101 (2002).
15. J. M. Schins, T. Schrama, J. Squier, G. J. Brakenhoff, and M. Müller, "Determination of material properties by use of third-harmonic generation microscopy," J. Opt. Soc. Am. B **19**, 1627–1634 (2002).
16. T. Y. F. Tsang, "Optical third-harmonic generation at interfaces," Phys. Rev. A **52**, 4116–4125 (1995).
17. J. Reintjes, *Nonlinear Optical Parametric Processes in Liquids and Gases* (Academic, 1984).
18. S.-W. Chu, S.-Y. Chen, T.-H. Tsai, T.-M. Liu, C.-Y. Lin, H.-J. Tsai, and C.-K. Sun, "*In vivo* developmental biology study using noninvasive multi-harmonic generation microscopy," Opt. Express **11**, 3093–3099 (2003).
19. M. Muller, J. Squier, K. R. Wilson, and G. J. Brakenhoff, "3D-microscopy of transparent objects using third harmonic generation," J. Microsc. **191**, 266–274 (1998).
20. V. Barzda, C. Greenhalgh, J. Aus der Au, J. Squier, S. Elmore, J. H. G. M. van Beek, "Second- and third-harmonic generation and multiphoton excitation fluorescence microscopy from simultaneous imaging of cardiomyocytes," in *Commerical and Biomedical Applications of Ultrafast Lasers IV*, J. Neev, C. B. Schaffer, and A. Ostendorf, eds., Proc. SPIE **5340**, 96–103 (2004).
21. A. C. Millard, P. W. Wiseman, D. N. Fittinghoff, K. Wilson, J. Squier, and M. Muller, "Third-harmonic generation microscopy by use of a compact, femtosecond fiber laser source," Appl. Opt. **38**, 7393–7397 (1999).
22. R. D. Schaller, J. C. Johnson, and R. J. Saykally, "Nonlinear chemical imaging microscopy: near-field third harmonic generation imaging of human blood cells," Anal. Chem. **72**, 5361–5364 (2000).
23. D. Debarre, W. Supatto, E. Farge, B. Moulia, M. C. Schanne-Klein, and E. Beaurepaire, "Velocimetric third-harmonic generation microscopy: micrometer-scale quantification of morphogenetic movements in unstained embryos," Opt. Lett. **29**, 2881–2883 (2004).
24. S. Y. Chen, A. Maksimichuk, E. Esarey, and D. Umstadter, "Observation of phase-matched relativistic harmonic generation," Phys. Rev. Lett. **84**, 5528–5531 (2000).
25. A. N. Naumov, D. A. Sidorov-Biryukov, A. B. Fedotov, and A. M. Zheltikov, "Third-harmonic generation in focused beams as a method of 3D microscopy of a laser-produced plasma," Opt. Spectrosc. **90**, 778–783 (2001).
26. S.-W. Chu, S.-Y. Chen, G.-W. Chern, T.-H. Tsai, Y.-C. Chen, B.-L. Lin, and C.-K. Sun, "Studies of C(2)/C(3) tensors in submicron-scaled bio-tissues by polarization harmonics optical microscopy," Biophys. J. **86**, 3914–3922 (2004).
27. C.-K. Sun, C.-C. Chen, S.-W. Chu, T.-H. Tsai, Y.-C. Chen, and B.-L. Lin, "Multiharmonic-generation biopsy of skin," Opt. Lett. **28**, 2488–2490 (2003).
28. D. A. Akimov, A. A. Ivanov, M. V. Alfimov, E. P. Grabchak, A. A. Shtykova, A. N. Petrov, A. A. Podshivalov, and A. M. Zheltikov, "J-aggregation visualized with two-photon resonant third-harmonic generation," J. Raman Spectrosc. **34**, 1007–1012 (2003).
29. T. Hasegawa, K. Ishikawa, T. Kanetake, T. Koda, K.

Takeda, H. Kobayashi, and K. Kubodera, "Excitonic resonant effect in the third-order nonlinear optical properties of blue- and red-form polydiacetylene films," Chem. Phys. Lett. **171**, 239–244 (1990).
30. R. D. Schaller, J. C. Johnson, K. R. Wilson, L. F. Lee, L. H. Haber, and R. J. Saykally, "Nonlinear chemical imaging nanomicroscopy: from second and third harmonic generation to multiplex (broad-bandwidth) sum frequency generation near-field scanning optical microscopy," J. Phys. Chem. B **106**, 5143–5154 (2002).
31. L. Canioni, S. Rivet, L. Sarger, R. Barille, P. Vacher, and P. Voisin, "Imaging of Ca^{2+} intracellular dynamics with a third-harmonic generation microscope," Opt. Lett. **26**, 515–517 (2001).
32. R. H. Hellwarth, "Third-order optical susceptibilities of liquids and solids," Prog. Quantum Electron. **5**, 1–68 (1977).
33. R. L. Swofford and A. C. Albrecht, "Nonlinear spectroscopy," Annu. Rev. Phys. Chem. **29**, 421–440 (1978).
34. T. Hasegawa, Y. Iwasa, H. Kishida, T. Koda, Y. Tokura, H. Tachibana, and Y. Kawabata, "Two-photon resonant third-harmonic generation in polysilanes," Phys. Rev. B **45**, 6317–6320 (1992).
35. M. A. Diaz-Garcia, F. Agullo-Lopez, W. E. Torruellas, and G. I. Stegeman, "Identification of two-photon states in phthalocyanines by third harmonic generation spectroscopy," Chem. Phys. Lett. **235**, 535–540 (1995).
36. P. R. Callis, "Two-photon induced fluorescence," Annu. Rev. Phys. Chem. **48**, 271–297 (1997).
37. A. Schulzgen, Y. Kawabe, E. Hanamura, A. Yamanaka, P. A. Blanche, J. Lee, H. Sato, M. Naito, N. T. Dan, S. Uchida, Y. Tanabe, and N. Peyghambarian, "Two-photon resonant third-harmonic generation in La_2CuO_4," Phys. Rev. Lett. **86**, 3164–3167 (2001).
38. A. B. Schumacher, J. S. Dodge, M. A. Carnahan, R. A. Kaindl, D. S. Chemla, and L. L. Miller, "Parity-forbidden excitation of $Si_2CuO_2Cl_2$ revealed by optical third-harmonic spectroscopy," Phys. Rev. Lett. **87**, 1–4 (2001).
39. P. D. Maker and R. W. Terhune, "Study of optical effects due to an induced polarization third order in the electric field strength," Phys. Rev. **137**, A801–A818 (1965).
40. J. Jerphagnon and S. K. Kurtz, "Maker fringes: a detailed comparison of theory and experiment for isotropic and uniaxial crystals," J. Appl. Phys. **41**, 1667–1681 (1970).
41. H. Tajalli, J. P. Jiang, J. T. Murray, N. R. Armstrong, A. Schmidt, M. Chandross, S. Maxumdar, and N. Peyghambarian, "Spectra of third-order optical nonlinear susceptibilities of epitaxial chloro-indium-phthalocyanines," Appl. Phys. Lett. **67**, 1639–1641 (1995).
42. R. R. Tykwinski, U. Gubler, R. E. Martin, F. Diederich, C. Bosshard, and P. Gunter, "Structure-property relationships in third-order nonlinear optical chromophores," J. Phys. Chem. B **102**, 4451–4465 (1998).
43. S. O. Konorov, D. A. Akimov, A. A. Ivanov, M. V. Alfimov, S. Botti, R. Ciardi, L. D. Deominicis, L. S. Asilyan, A. A. Podshivalov, D. A. Sidorov-Biryukov, R. Fantoni, and A. M. Zheltikov, "Femtosecond optical harmonic generation as a non-linear spectroscopic probe for carbon nanotubes," J. Raman Spectrosc. **34**, 1018–1024 (2003).
44. W. E. Torruellas, D. Neher, R. Zanoni, G. I. Stegeman, F. Kajzar, and M. Leclerc, "Dispersion measurements of the third-order nonlinear susceptiblity of polythiophene thin films," Chem. Phys. Lett. **175**, 11–16 (1990).
45. J. C. Baumert, G. C. Bjorklund, D. H. Jundt, M. C. Jurich, H. Looser, R. D. Miller, J. Rabolt, R. Sooriyakumaran, J. D. Swalen, and R. J. Twieg, "Temperature dependence of the third-order nonlinear optical susceptibilities in polysilanes and polygermanes," Appl. Phys. Lett. **53**, 1147–1149 (1988).
46. C. Halvorson, R. Wu, D. Moses, F. Wudl, and A. J. Heeger, "Third harmonic generation spectra of degenerate ground state derivatives of poly(1,6-heptadiyne)," Chem. Phys. Lett. **212**, 85–89 (1993).
47. J. McElvain, M. Cha, H. Yu, N. Zhang, F. Wudl, and A. J. Heeger, "Third harmonic generation spectrum of a degenerate ground state conjugated polymer. Direct evidence of simultaneous two- and three-photon resonance," Chem. Phys. Lett. **247**, 221–226 (1995).
48. H. S. Nalwa, M. Hanack, G. Pawlowski, and M. K. Engel, "Third-order nonlinear optical properties of porphyrazine phthalocyanine and naphthalocyanine germanium derivities: demonstrating the effect of pi-conjugation length on third-order optical nonlinearity of two-dimensional molecules," Chem. Phys. **245**, 17–26 (1999).
49. S. R. Marder, J. W. Perry, G. Bourhill, C. B. Gorman, B. G. Tiemann, and K. Mansour, "Relation between bond-length alternation and second electronic hyperpolarizability of conjugated molecules," Science **261**, 186–189 (1993).
50. J. Y. Huang and M. H. Wu, "Nonlinear optical studies of binary mixtures of hydrogen bonded liquids," Phys. Rev. E **50**, 3737–3746 (1994).
51. I. Ledoux, I. D. W. Samuel, J. Zyss, S. N. Yaliraki, F. J. Schattenmann, R. R. Schrock, and R. J. Silbey, "Third-order microscopic nonlinearities of very long chain polyenes: saturation phenomena and conformational effects," Chem. Phys. **245**, 1–16 (1999).
52. R. Barille, L. Canioni, S. Rivet, L. Sarger, and G. Rivoire, "Nonlinearity measurements of thin films by third-harmonic-generation microscopy," Phys. Rev. E **66**, 067062, 1–4 (2002).
53. G. R. Meredith, B. Buchalter, and C. Hanzlik, "Third-order optical susceptibility determination by third harmonic generation. 2," J. Phys. Chem. **78**, 1543–1551 (1983).
54. V. Shcheslavskiy, G. Petrov, and V. V. Yakovlev, "Nonlinear optical susceptibility measurements of solutions using third-harmonic generation on the interface," Appl. Phys. Lett. **82**, 3982–3984 (2003).
55. T. Tsang, "Third- and fifth-harmonic generation at the interfaces of glass and liquids," Phys. Rev. A **54**, 5454–5457 (1996).
56. P. Lemberg and J. W. Legge, *Hematin Compounds and Bile Pigments* (Interscience, 1949).
57. R. B. Boyd, *Nonlinear Optics*, 2nd ed. (Academic, 2003).
58. E. J. Sanchez, L. Novotny, G. R. Holtom, and X. S. Xie, "Room-temperature fluorescence imaging and spectroscopy of single molecules by two-photon excitation," J. Phys. Chem. A **101**, 7019–7023 (1997).
59. C. Bosshard, U. Gubler, P. Kaatz, W. Mazerant, and U. Meier, "Non-phase-matched optical third-harmonic generation in noncentrosymmetric media: cascaded second-order contributions for the calibration of third-order nonlinearities," Phys. Rev. B **61**, 10688–10701 (2000).
60. C. Wang, "Empirical relation between the linear and the third-order nonlinear optical susceptibilities," Phys. Rev. B **2**, 2045–2048 (1970).
61. N. Sugimoto, H. Kanbara, S. Fujiwara, K. Tanaka, and Y. Shimizugawa, "Third-order optical nonlinearities and their ultrafast response in Bi_2O_3—B_2O_3—SiO_2 glasses," J. Opt. Soc. Am. B **16**, 1904–1908 (1999).
62. N. L. Boling, A. J. Glass, and A. Owyoung, "Empirical relationships for predicting nonlinear refractive index changes in optical solids," IEEE J. Quantum Electron. **QE-14**, 601–608 (1978).
63. R. W. Boyd, *Nonlinear Optics* (Academic, 1992).
64. J. R. Heflin, Y. M. Cai, and A. F. Garito, "Dispersion measurements of electric-field-induced second-harmonic generation and third-harmonic generation in conjugated linear chains," J. Opt. Soc. Am. B **8**, 2132–2147 (1991).
65. U. Gubler and C. Bosshard, "Optical third-harmonic generation of fused silica in gas atmosphere: absolute value of the third-order nonlinear susceptibility $\chi^{(3)}$," Phys. Rev. B **61**, 10702–10710 (2000).
66. F. Kajzar and J. Messier, "Third-harmonic generation in liquids," Phys. Rev. A **32**, 2352–2363 (1985).
67. G. R. Meredith, B. Buchalter, and C. Hanzlik, "Third-order optical susceptibility determination by third harmonic generation. 1," J. Chem. Phys. **78**, 1533–1542 (1983).
68. P. S. Tsai, N. Nishimura, E. J. Yoder, E. M. Dolnick, G. A. White, and D. Kleinfeld, "Principles, design, and construction of a two photon laser scanning microscope for

in vitro and *in vivo* brain imaging," in *In Vivo Optical Imaging of Brain Function*, R. D. Frostig, ed. (CRC Press, 2002), pp. 113–171.
69. D. J. Segelstein, "The complex refractive index of water," M.S. thesis (University of Missouri, Kansas City, 1981).
70. K. I. Hildrum, T. Isaksson, T. Naes, and A. Tandberg, *Near Infra-red Spectroscopy: Bridging the Gap between Data Analysis and NIR Applications*, Ellis Horwood Series in Analytical Chemistry (Ellis Horwood, 1992), p. 473.
71. K. Murayama, B. Yuan, Y. Ozaki, M. Tomida, and S. Era, "Near-infrared spectroscopy for liquids of microliter volume using capillaries with wall transmission," Analyst (Cambridge, U.K.) **128**, 957–959 (2003).
72. H. EI-Kashef, "Study of the refractive properties of laser dye solvents: toluene, carbon disulphide, chloroform, and benzene," Opt. Mater. (Amsterdam, Neth.) **20**, 81–86 (2002).
73. B. Halle and M. Davidovic, "Biomolecular hydration: from water dynamics to hydrodynamics," Proc. Natl. Acad. Sci. U.S.A. **100**, 12135–12140 (2003).
74. J. L. Dela Cruz and G. J. Blanchard, "The influence of chromophore structure on intermolecular interactions. A study of selected rhodamines in polar protic and aprotic solvents," J. Phys. Chem. A **106**, 10718–10724 (2002).
75. G. R. Fleming and M. Cho, "Chromophore-solvent dynamics," Annu. Rev. Phys. Chem. **47**, 109–134 (1996).
76. A. Bondi, "van der Waals volumes and radii," J. Phys. Chem. **68**, 441–451 (1964).
77. H. T. Edward, "Molecular volumes and the Stokes–Einstein equation," J. Chem. Educ. **47**, 261–270 (1970).
78. J. E. Selwyn and J. I. Steinfeld, "Aggregation equilibria of xanthene dyes," J. Phys. Chem. **76**, 762–774 (1971).
79. F. L. Arbelo, P. R. Ojeda, and I. L. Arbeloa, "On the aggregation of rhodamine B in ethanol," Chem. Phys. Lett. **148**, 253–258 (1988).
80. H. G. Elias, *Makromolekule* (Wiley-VCH, 1990).
81. D. Arosio, H. E. Kwansa, H. Gering, G. Piszczek, and E. Bucci, "Static and dynamic light scattering approach to the hydration of hemoglobin and its supertetramers in the presence of osmolites," Biopolymers **63**, 1–11 (2002).
82. B. F. Levine and C. G. Bethea, "Molecular hyperpolarizabilities determined from conjugated and nonconjugated organic liquids," Appl. Phys. Lett. **24**, 445–447 (1973).
83. H. Reis, M. G. Papadopoulos, and D. N. Theodorou, "Calculation of refractive indices and third-harmonic generation susceptibilities of liquid benzene and water: comparison of continuum and discrete local-field theories," J. Phys. Chem. **114**, 876–881 (2000).
84. C. Xu and W. W. Webb, "Measurement of two-photon excitation cross sections of molecular fluorophores with data from 690 to 1050 nm," J. Opt. Soc. Am. B **13**, 481–491 (1996).
85. D. L. Wokosin, C. M. Loughrey, and G. L. Smith, "Characterization of a range of Fura dyes with two-photon excitation," Biophys. J. **86**, 1726–1738 (2004).
86. C. Xu, R. M. Williams, W. Zipfel, and W. W. Webb, "Multiphoton excitation cross-sections of molecular fluorophores," Bioimaging **4**, 198–207 (1996).
87. C. Xu, W. Zipfel, J. B. Shear, R. M. Williams, and W. W. Webb, "Multiphoton fluorescence excitation: new spectral windows for biological nonlinear microscopy," Proc. Natl. Acad. Sci. U.S.A. **93**, 10763–10768 (1996).
88. W. Orttung and J. Warner, "Refractive index dispersion in equine hemoglobin solutions," J. Phys. Chem. **69**, 3188–3190 (1965).
89. D. Faber, E. G. Mik, A. Aalders, and T. G. van Leeuwen, "Oxygen saturation dependent index of refraction of hemoglobin solutions assessed by OCT," in *Coherence Domain Optical Methods and Optical Coherence Tomography in Biomedical VII*, V. Tuchin, J. Izatt, and J. Fujimoto, eds., Proc. SPIE **4956**, 271–281 (2003).
90. X. Quan and E. Fry, "Empirical equation for the index of refraction of seawater," Appl. Opt. **34**, 3477–3480 (1995).
91. L. V. Butov, A. Zrenner, G. Abstreiter, A. V. Petinova, and K. Eberl, "Direct and indirect magnetoexcitons in symmetrical $ln_xAg_{1-x}As/GaAs$ coupled quantum wells," Phys. Rev. B **52**, 12153–12157 (1995).
92. M. L. Ferrer, R. Duchowicz, B. Carrasco, J. G. de la Torre, and A. U. Acuñ, "The conformation of serum albumin in solution: a combined phosphorescence depolarization-hydrodymic modeling study," Biophys. J. **80**, 2422–2430 (2001).
93. T. Lazaridis, "Solvent reorganization energy and entropy in hydrophobic hydration," J. Phys. Chem. B **104**, 4964–4979 (2000).
94. K. E. S. Tang and V. A. Bloomfield, "Excluded volume in solvation: sensitivity of scaled-particle theory to solvent size and density," Biophys. J. **79**, 2222–2234 (2000).
95. C. E. Giacomelli, M. J. Esplandiu, P. I. Ortiz, M. J. Avena, and C. P. De Pauli, "Ellipsometric study of bovine serum albumin adsorped onto Ti/TiO_2 electrodes," J. Colloid Interface Sci. **218**, 404–411 (1999).
96. A. Samokhvalov and R. Naaman, "Wavelength- and time-dependent two-photon photoemission spectroscopy of dye-coated silicon surface," J. Phys. Chem. B **104**, 11248–11252 (2000).
97. W. P. de Boeij, M. S. Pshenichnikov, and D. A. Wiersma, "Ultrafast solvation dynamics explored by femtosecond photon echo spectroscopies," Annu. Rev. Phys. Chem. **49**, 99–123 (1998).
98. A. B. Myers, "Molecular electronic spectral broadening in liquids and glasses," Annu. Rev. Phys. Chem. **49**, 267–295 (1998).
99. P. Vohringer, D. C. Arnett, R. A. Westervelt, M. J. Feldstein, and N. F. Scherer, "Optical dephasing on femtosecond time scales: direct measurement and calculation from solvent spectral densities," J. Chem. Phys. **102**, 4027–4036 (1994).
100. M. Sinclair, D. Moses, K. Akagi, and A. J. Heeger, "Anisotropy of the third-order nonlinear-optical susceptibility in a degenerate-ground-state conjugated polymer: *trans*-$(CH)_x$," Phys. Rev. B **38**, 10724–10733 (1988).
101. V. Shcheslavskiy, G. I. Petrov, S. Saltiel, and V. V. Yakovlev, "Quantitative characterization of aqueous solutions probed by the third-harmonic generation microscopy," J. Struct. Biol. **147**, 42–49 (2004).
102. A. H. Buist, M. Muller, R. I. Ghauharali, G. J. Brakenhoff, J. A. Squier, C. J. Bardeen, V. V. Yakeovlev, and K. R. Wilson, "Probing microscopic chemical environments with high-intensity chirped pulses," Opt. Lett. **24**, 244–246 (1999).
103. J. A. Squier, K. R. Wilson, V. V. Yakovlev, C. Bardeen, A. Buist, M. Muller, and G. J. Brakenhoff, "Effect of pulse phase and shape on the efficiency of multiphoton processes: implications for fluorescence microscopy," in *Conference on Lasers and Electro-Optics (CLEO/US)* (Optical Society of America, 1999), p. 80.
104. H. Kawano, Y. Nabekawa, A. Suda, Y. Oishi, H. Mizuno, A. Miyawaki, and K. Midorikawa, "Attenuation of photobleaching in two-photon excitation fluorescence from green fluorescent protein with shaped excitation pulses," Biochem. Biophys. Res. Commun. **11**, 592–596 (2003).
105. F. Kajzar and J. Messier, "Original technique for third-harmonic-generation measurements in liquids," Rev. Sci. Instrum. **58**, 2081–2085 (1987).
106. I. E. Borissevitch, N. Rakov, G. S. Maciel, and C. B. de Araujo, "Changes in porphyrin nonlinear absorption owing to interaction with bovine serum albumin," Appl. Opt. **39**, 4431–4435 (2000).
107. D. Kleinfeld, P. P. Mitra, F. Helmchen, and W. Denk, "Fluctuations and stimulus-induced changes in blood flow observed in individual capillaries in layers 2 through 4 of rat neocortex," Proc. Natl. Acad. Sci. U.S.A. **95**, 15741–15746 (1998).
108. E. Chaigneau, M. Oheim, E. Audinat, and S. Charpak, "Two-photon imaging of capillary blood flow in olfactory

bulb glomeruli," Proc. Natl. Acad. Sci. U.S.A. **100**, 13081–13086 (2003).
109. I. H. Malitson, "Interspecimen comparison of refractive index of fused silica," J. Opt. Soc. Am. **55**, 1205–1209 (1965).
110. Edmund Industrial Optics, "Glass Materials Table," www.edmundoptics.com, ed. (2001).
111. J. M. Resa, C. Gonzalez, S. O. de Landaluce, and J. Lanz, "Densities, excess molar volumes, and refractive indices of ethyl acetate and aromatic hydrocarbon binary mixtures," J. Chem. Thermodyn. **34**, 995–1004 (2002).
112. P. D. T. Huibers, "Models for the wavelength dependence of the index of refraction of water," Appl. Opt. **36**, 3785–3787 (1997).
113. S. Yaltkaya and R. Aydin, "Experimental investigation of temperature effect on the refractive index of dye laser solutions," Turk. J. Phys. **26**, 41–47 (2002).
114. G. E. Perlmann, L. G. Longsworth, "The specific refractive increment of some purified proteins," J. Am. Chem. Soc. **70**, 2719–2724 (1948).
115. H. J. Coles, B. R. Jennings, and V. J. Morris, "Refractive index increment measurement for bacterial suspensions," Phys. Med. Biol. **20**, 310–313 (1975).
116. M. Halwer, G. C. Nutting, and B. A. Brice, "Molecular weight of lactoglobulin, ovalbumin, lysozyme and serum albumin by light scattering," J. Am. Chem. Soc. **73**, 2786–2790 (1951).
117. J. Noack, D. X. Hammer, G. D. Noojin, B. A. Rockwell, and A. Vogel, "Influence of pulse duration on mechanical effects after laser-induced breakdown in water," J. Appl. Phys. **83**, 7488–7495 (1998).
118. P. Latimer, "Anomalous dispersion of CS_2 and $ChCl_3$: theoretical predictions," J. Opt. Soc. Am. **51**, 116–118 (1961).
119. E. M. Vogel, S. G. Kosinski, D. M. Krol, J. L. Jackel, S. R. Friberg, M. K. Oliver, and J. D. Powers, "Structural and optical study of silicate glasses for nonlinear optical devices," J. Non-Cryst. Solids **107**, 244–250 (1989).
120. H. Nasu, J. Matsuoka, and K. Kanichi, "Second- and third-order optical non-linearity of homogeneous glasses," J. Non-Cryst. Solids **178**, 23–30 (1994).
121. D. W. Hall, M. A. Newhouse, N. F. Borrelli, W. H. Dumbaugh, and D. L. Weidman, "Nonlinear optical susceptibilities of high-index glasses," Appl. Phys. Lett. **54**, 1293–1295 (1989).